Structural Safety 112 (2025) 102536

Contents lists available at ScienceDirect

Structural Safety

journal homepage: www.elsevier.com/locate/strusafe

Improved Bayesian model updating of geomaterial parameters for slope reliability assessment considering spatial variability

Shui-Hua Jiang [a], Hong-Peng Hu [a], Ze Zhou Wang [b,*]

[a] School of Infrastructure Engineering, Nanchang University, 999 Xuefu Road, Nanchang 330031, China
[b] Civil Engineering Division, Department of Engineering, University of Cambridge, 7a JJ Thomson Avenue, Cambridge CB3 0FA, United Kingdom

ARTICLE INFO

Keywords:
Slope
Spatial variability
Likelihood function
Bayesian model updating
Subset simulation
Reliability assessment

ABSTRACT

In engineering practice, Bayesian model updating using field data is often conducted to reduce the substantial inherent epistemic uncertainties in geomaterial properties resulting from complex geological processes. The Bayesian Updating with Subset simulation (BUS) method is commonly employed for this purpose. However, the wealth of field data available for engineers to interpret can lead to challenges associated with the "curse of dimensionality". Specifically, the value of the likelihood function in the BUS method can become extremely small as the volume of field data increases, potentially falling below the accuracy threshold of computer floating-point operations. This undermines both the computational efficiency and accuracy of Bayesian model updating. To effectively address this technical challenge, this paper proposes an improved BUS method developed based on parallel system reliability analysis. Leveraging the Cholesky decomposition-based midpoint method, the total failure domain in the original BUS method, which involves a low acceptance rate, is subdivided into several sub-failure domains with a high acceptance rate. Facilitated with an improved Metropolis-Hastings algorithm, the improved BUS method enables the consideration of a large volume of field data and spatial variability of geomaterial properties in the probabilistic back analysis. The results of an illustrative soil slope, involving spatially variable undrained shear strength, demonstrate that the improved BUS method is effective in simultaneously incorporating a substantial volume of field measurements and observations in the model updating process. Through a comparison with the original BUS method, the improved BUS method is shown to be useful for Bayesian model updating of high-dimensional spatially variable geomaterial properties and slope reliability assessment.

1. Introduction

Due to complex geological, chemical, physical, and environmental processes, as well as human activities, there exists site-specific inherent, statistical, and model uncertainties in geomaterial properties. Therefore, accurately estimating the statistical information in geomaterial properties, including mean, standard deviation, and spatial correlation, is crucial for geotechnical engineering applications (e.g., [6,20,33]). Bayesian model updating that fuses prior engineering knowledge and statistical information as well as the wealth of available field data is commonly employed to infer the site-specific statistics of geomaterial properties, thereby providing crucial information for slope reliability assessment (e.g., [11,28]).

In existing literature, various methods have been developed for this purpose. For example, Deng and Lee [7] proposed a back analysis framework involving the combination of error backpropagation neural networks and a genetic algorithm and demonstrated the effectiveness using the displacement monitoring data of the Three Gorges Project. Furthermore, Harris et al. [14] used the field measurements of soil water content in a rainfall-induced failed slope in New Zealand to calibrate the associated numerical model for seepage analysis. Wang et al. [38] employed the maximum likelihood method to back analyze the shear strength of the geomaterials and the anchor force of the North No. 3 Highway in Taiwan. However, these studies all employed deterministic modeling and a limited set of field measurements, thereby not providing reliable statistical information of the geomaterial properties under study.

In contrast, probabilistic back analysis that can yield statistical outputs is preferred in engineering practice. In particular, Bayesian model updating can effectively perform the task by combining the prior

* Corresponding author.
E-mail addresses: wangzz@u.nus.edu, zw437@cam.ac.uk (Z.Z. Wang).

https://doi.org/10.1016/j.strusafe.2024.102536
Received 28 March 2024; Received in revised form 5 September 2024; Accepted 10 September 2024
Available online 14 September 2024

engineering and statistical knowledge with field data (e.g., [31]), thereby permitting subsequent reliability assessments of the engineering system under study. For example, Jiang et al. [17] successfully updated the probability distributions of soil properties based on limited field data using Bayesian model updating for slope reliability assessment. Similarly, Sun et al. [37] employed the Markov Chain Monte Carlo (MCMC) simulation to probabilistically back analyze the statistical distributions of rock mass properties based on multiple types of field monitoring data. Ouyang and Liu [30] further advanced Bayesian model updating through integrating conditional random fields into the Bayesian Updating with Subset simulation (BUS) method, and probabilistically back analyzed soil properties for slope reliability assessment using multiple types of field data. Liu et al. [27] developed a Bayesian-based slope digital twin model and used slope monitoring data and past performance records to optimize the selection of slope hydraulic model for updating the statistical information of soil properties. Zhang et al. [45] integrated the polynomial chaos expansion technique, coupled hydro-mechanical modeling, and MCMC simulation into an efficient probabilistic parameter estimation method for coupled hydro-mechanical behavior in soil slopes.

Although Bayesian model updating has been successfully implemented by these studies, the method can encounter the "curse of dimensionality" that arises from (i) high-dimensional parameter space, and (ii) high-dimensional likelihood function caused by the consideration of a substantial volume of field data (e.g., [29,28]. In the context of this paper, high-dimensional parameter space refers to the need of using a large number of random variables to describe the spatial variability of geomaterial properties, which can be a challenging task for traditional Bayesian model updating (e.g., [4,19,20]). For example, the MCMC method commonly used in traditional Bayesian model updating may not only experience a surge in computational demand but also face difficulties in ensuring the stability and convergence of the Markov chain (e.g., [5,24,12]). Although the BUS method proposed by Straub and Papaioannou [36] partially addressed the instability issue in the Markov chain and improved the handling of high-dimensional parameter space (e.g., [36,10,16]), the issue of high-dimensional likelihood function remain unsolved. When incorporating a large amount of field data, the likelihood function values become extremely small, even below the precision of computer floating-point operations. The resulting low acceptance rate in the BUS method then leads to a sharp increase in computational costs (e.g., [28,30,41,43]). Given this limitation, there is a need for a strategy to permit the incorporation of a large volume of field data and avoid the instability of Bayesian model updating caused by the extremely small likelihood function values (e.g., [9]).

This paper proposes an improved BUS method for handling non-Gaussian random fields of geomaterial parameters. Using the Cholesky decomposition-based midpoint method, the likelihood function constructed based on a large number of field data is first subdivided into several sub-likelihood functions. This transformation converts the original Bayesian model updating problem into several parallel problems containing individual limit state functions. Facilitated with an improved Metropolis-Hastings algorithm, the improved BUS method then sequentially solves the equivalent structural reliability problem associated with each sub-likelihood function, enabling efficient Bayesian model updating of geomaterial parameters for slope reliability assessment in the face of massive field data.

2. Background

As highlighted in the introduction, this paper proposes an improved method for Bayesian model updating of spatially variable geomaterial parameters utilizing extensive field data. The proposed method is developed based on the following two key techniques: (i) random field modeling of spatial variability, and (ii) Bayesian model updating. Specifically, the random field theory is used to characterize the spatial variability of geomaterial parameters in numerical calculations, while Bayesian model updating is employed to incorporate extensive field data and infer the distribution of geomaterial parameters. In the following parts of this section, the background information pertaining to these key techniques is explained.

2.1. Simulation of non-Gaussian random fields

Geomaterial parameters are typically observed to exhibit spatial variability [20,33,47]. In geotechnical engineering, geomaterials primarily refer to soil and rock masses. The geomaterial parameters includes, but not limited to, shear strength parameters (e.g., undrained shear strength, cohesion and friction angle), hydraulic parameters (e.g., permeability coefficient, saturated and residual water contents and soil water characteristic curve fitting parameters) and stiffness parameters (e.g., modulus of elasticity, Poisson's ratio). Moreover, these geomaterial parameters do not often follow Gaussian distributions, and cross-correlations exist among these parameters (e.g., [46]). Therefore, non-Gaussian random fields are commonly employed to simulate their spatial autocorrelation (e.g., [23,21]). The Cholesky decomposition-based midpoint method is often employed for generating non-Gaussian random fields, and its implementation procedures are summarized as follows (e.g., [42,26]):

(i) Divide the model domain into random field elements and extract the coordinates of the centroid of each grid, $Q_i = (x_i, y_i)$, where $i = 1, 2, 3, \cdots, l$, and l is the number of elements in the model domain.
(ii) Calculate the autocorrelation coefficient ρ_{ij} and form the autocorrelation matrix $\boldsymbol{\rho}$. Perform Cholesky decomposition, $\mathscr{L}\mathscr{L}^{\mathrm{T}} = \boldsymbol{\rho}$, to obtain the lower triangular matrix $\mathscr{L}$ of dimension $l \times l$.
(iii) Generate independent standard normal random sample matrix $\boldsymbol{\xi}$ with dimension $n \times l$, where n is the number of random field realizations.
(iv) Multiply the matrix $\boldsymbol{\xi}$ by the upper triangular matrix $\mathscr{L}^{\mathrm{T}}$, $\boldsymbol{\chi}^D = \boldsymbol{\xi}\mathscr{L}^{\mathrm{T}}$, and obtain a correlated standard normal random sample matrix $\boldsymbol{\chi}^D$ with dimension $n \times l$.
(v) Depending on the statistical characteristics of the parameters, use the Nataf transformation (e.g., [25]) to convert the correlated standard normal sample matrix $\boldsymbol{\chi}^D$ into a non-Gaussian random field realization $\boldsymbol{H}$. The following is given by

$$\begin{bmatrix} H_{1,1} & H_{1,2} & \cdots & H_{1,l} \\ H_{2,1} & H_{2,2} & \cdots & H_{2,l} \\ \vdots & \vdots & \ddots & \vdots \\ H_{n,1} & H_{n,2} & \cdots & H_{n,l} \end{bmatrix} = T\left\{ \begin{bmatrix} \xi_{1,1} & \xi_{1,2} & \cdots & \xi_{1,l} \\ \xi_{2,1} & \xi_{2,2} & \cdots & \xi_{2,l} \\ \vdots & \vdots & \ddots & \vdots \\ \xi_{n,1} & \xi_{n,2} & \cdots & \xi_{n,l} \end{bmatrix} \begin{bmatrix} \mathscr{L}_{1,1} & \mathscr{L}_{1,2} & \cdots & \mathscr{L}_{1,l} \\ 0 & \mathscr{L}_{2,2} & \cdots & \mathscr{L}_{2,l} \\ \vdots & \vdots & \ddots & \vdots \\ 0 & 0 & \cdots & \mathscr{L}_{l,l} \end{bmatrix} \right\} \tag{1}$$

where $T(.)$ refers to the Nataf transformation (e.g., [25]).

2.2. Bayesian model updating

Bayesian model updating can infer the statistical information of geomaterial parameters such as shear strength parameters, hydraulic parameters, and stiffness parameters, among others using limited field data, and this process is executed through the estimation of the posterior probability density function (PDF) of the parameters (e.g., [36]). In this study, only the undrained shear strength is considered although Bayesian model updating can be used to infer the distribution of a range of geomaterial parameters depending on the calculation model and the nature of field observations. According to the Bayes' theorem, the posterior PDF is calculated as follows (e.g., [1]):

$$f'_X(\boldsymbol{x}) = aL(\boldsymbol{x})f'_X(\boldsymbol{x}) \tag{2}$$

where $f'_X(\boldsymbol{x})$ and $f''_X(\boldsymbol{x})$ are, respectively, the prior and posterior PDFs of geomaterial parameters $\boldsymbol{X}$,$\boldsymbol{X} = (X_1, X_2, \cdots, X_N)^{\mathrm{T}}$, and N is the number of

random variables, which equals l for a single-parameter random field; $\boldsymbol{x}$ is a realization of $\boldsymbol{X}$; a is a normalization constant to ensure that integral of $f'_X(\boldsymbol{x})$ over the probabilistic domain Ω of $\boldsymbol{X}$ is equal to 1, $a = 1/\int_\Omega L(\boldsymbol{x}) f'_X(\boldsymbol{x}) d\boldsymbol{x}$; $L(\boldsymbol{x})$ is the likelihood function.

Through defining a new failure domain Ω_{acc}, the BUS method transforms the Bayesian model updating problem into an equivalent structural reliability problem (e.g., [36]):

$$\Omega_{acc} = \{G(\boldsymbol{x}) = U - cL(\boldsymbol{x}) \le 0\} \tag{3}$$

where U is a uniformly distributed random variable in the interval [0, 1.0]; c is the multiplier of the likelihood function, which needs to ensure that for any parameters $\boldsymbol{X}$, $cL(\boldsymbol{x}) \le 1.0$. Subset simulation [3,32] is then employed to solve this equivalent structural reliability problem. Following Betz et al. [4], the constant c, a key parameter for the Bayesian model updating, is chosen adaptively as the reciprocal of the maximum of the likelihood function values over the samples at the current subset simulation level, i.e.

$$c_i = \frac{1}{\max\left[c_{i-1}^{-1}, \{L(\boldsymbol{x}_{i,k}), k = 1, 2, \cdots, n\}\right]} (i = 1, 2, \cdots, s) \tag{4}$$

where n is the number of samples at each subset simulation level; s is the number of simulation levels required to reach the failure domain; c_{i-1} is the constant evaluated at simulation level i–1.

In addition, to fully utilize on-site experimental data, monitoring data, observation data, and any relevant field data to update the probability distributions of geomaterial parameters, it is necessary to first construct a likelihood function based on the various types of field information, which is a crucial step in Bayesian model updating (e.g., [16]). Conceptually, the likelihood function represents the probability of the occurrence of a field information Z given that the uncertain parameters $\boldsymbol{X}$ take a specific value $\boldsymbol{x}$. Mathematically, it is expressed as follows:

$$L(\boldsymbol{x}) \propto P(Z|\boldsymbol{X} = \boldsymbol{x}) \tag{5}$$

where $P(.)$ is the probability of an event; Z is the field event.

Furthermore, due to the limitations in the precision of instruments and experiment apparatus, human errors, or any other random errors, measurement errors are inevitable. Therefore, measurement errors are typically considered as additional uncertainties, which are added to the simulated values of geomaterial parameters. Mathematically, the k-th set of on-site or laboratory test data can be represented as $x_k^m = x_k + \varepsilon_k$, and the corresponding likelihood function is given by (e.g., [35]):

$$L(x_k) = f_\varepsilon(x_k^m - x_k) \tag{6}$$

where $f_\mathcal{E}(.)$ is the PDF of measurement error ε_k.

In addition, it is also feasible to treat the measurement error as a multiplier, and the k-th set of on-site or laboratory test data can be represented as $x_k^m = x_k \varepsilon_k$, and the corresponding likelihood function is given by (e.g., [36])

$$L(x_k) = f_\varepsilon\left(\frac{x_k^m}{x_k}\right) \tag{7}$$

In general, the formulation of the likelihood function depends on the type of field information. For direct information, such as on-site or laboratory test data, it is commonly assumed that the data obtained through different test methods are independent. Following the concept in Eq. (5), the measurement error ε_k typically follows a normal distribution with a mean of zero and a standard deviation of σ_ε. The corresponding likelihood function can be constructed as follows:

$$L(\boldsymbol{x}) = \alpha \prod_{k=1}^{n_d} \exp\left[-\frac{(x_k^m - x_k)^2}{2\sigma_\varepsilon^2}\right] \tag{8}$$

where α is a normalization constant, $\alpha = \left(2\pi\sigma_\varepsilon^2\right)^{-n_d/2}$, $k = 1, 2, \cdots, n_d$, where n_d is the number of field samples.

3. Improved BUS method

3.1. Division of failure domain

It is readily observed in Eq. (8) that as the number of field data (n_d) increases, the likelihood function value exponentially decreases, resulting in a very small failure domain Ω_{acc} and a very low acceptance rate in the original BUS method. As a result, a very large number of repeated samples will be generated, which can significantly affect the accuracy and consistency of the estimated posterior distributions even though a large sample size is used in each subset simulation level. In this regard, the improved BUS method proposed in this paper overcomes this issue by subdividing the original likelihood function $L(\boldsymbol{x})$ with a low acceptance rate into several sub-likelihood functions $W(\boldsymbol{x})$ with a high acceptance rate. This configuration transforms a reliability problem with a small failure region into a parallel system reliability problem with multiple larger failure regions. As a result, Eq. (8) can be revised as

$$L(\boldsymbol{x}) = \prod_{k=1}^{n_d} W_k(\boldsymbol{x}) \tag{9}$$

where $W_k(\boldsymbol{x})$ is the likelihood function constructed using the k-th set of field data; n_d is the number of sub-likelihood functions, which is also equal to the number of field samples.

While multiple sets of field data can also be used to construct a single sub-likelihood function, in this paper, each sub-likelihood function is constructed using only one set of field data. Subsequently, following the strategy adopted in the original BUS method, a set of uniformly distributed random variables U_k in the interval [0, 1.0] are introduced, and several different failure domains Ω_{acc}^k can be constructed as follows:

$$\Omega_{acc}^k = \{g_k(\boldsymbol{x}) = U_k - c_k W_k(\boldsymbol{x}) \le 0\} \tag{10}$$

where c_k is the multiplier of the corresponding sub-likelihood function $W_k(\boldsymbol{x})$. Referring to the principles of the BUS method, it should be ensured that for any parameters $\boldsymbol{X}$, $c_k W_k(\boldsymbol{x}) \le 1.0$. Similarly, the value of c_k can be determined according to Eq. (4).

In a nutshell, in contrast to the original BUS method, the improved BUS method proposed in this paper subdivides the original failure domain Ω_{acc} with a low acceptance rate into several sub-failure domains Ω_{acc} with a high acceptance rate as follows:

$$\begin{aligned} \Omega_{acc} &= \left[\Omega_{acc}^1 \cap \Omega_{acc}^2 \cdots \cap \Omega_{acc}^{n_d}\right] \\ &= \left[\max\{U_k - c_k W_k(\boldsymbol{x})\} \le 0\right], k = 1, 2, \cdots, n_d \end{aligned} \tag{11}$$

3.2. Implementation procedures

In this section, the implementation procedures of the proposed improved BUS method are explained using the undrained shear strength (s_u) data as the example. The first step involves the construction of a likelihood function as follows:

$$L(\boldsymbol{x}) = \alpha \prod_{k=1}^{n_d} \exp\left\{-\frac{\left[s_{u_k}^m - s_{u_{j,\boldsymbol{h}(k)}}\right]^2}{2\sigma_\varepsilon^2}\right\} \tag{12}$$

where α is a normalization constant, $\alpha = \left(2\pi\sigma_\varepsilon^2\right)^{-n_d/2}$; j refers to the j-th random field realization; $\boldsymbol{h}$ is the vector containing the coordinate indices of the n_d field samples, and $\boldsymbol{h}(k)$ refers to the coordinate index of the k-th field sample in the random field domain. Therefore, $s_{u_k}^m$ is the measured undrained shear strength at the location of the k-th field sample, and $s_{u_{j,\boldsymbol{h}(k)}}$ is the simulated undrained shear strength data at the location of the k-th field sample for the j-th random field realization.

Referring to Eq. (1), $s_{u_{j,\boldsymbol{h}(k)}}$ can be calculated as follows:

$$s_{u_{j,\boldsymbol{h}(k)}} = H_{j,\boldsymbol{h}(k)} = T\left(\xi_{j,1}\mathscr{L}_{1,\boldsymbol{h}(k)} + \xi_{j,2}\mathscr{L}_{2,\boldsymbol{h}(k)} + \cdots + \xi_{j,\boldsymbol{h}(k)}\mathscr{L}_{\boldsymbol{h}(k),\boldsymbol{h}(k)}\right) \tag{13}$$

To improve the computational efficiency of Bayesian model updating, the coordinate indices of the n_d field samples are set as 1, 2, ⋯, n_d, in sequence, namely $\boldsymbol{h}(k) = k$, $k = 1, 2, \cdots, n_d$. In this way, Eq. (13) can be rewritten as

$$s_{u_{j,\boldsymbol{h}(k)}} = s_{u_{j,k}} = H_{j,k} = T(\xi_{j,1}\mathscr{L}_{1,k} + \xi_{j,2}\mathscr{L}_{2,k} + \cdots + \xi_{j,k}\mathscr{L}_{k,k}) \tag{14}$$

Eq. (14) can be further written in the matrix form as follows:

$$\begin{bmatrix} s_{u_{1,1}} & s_{u_{1,2}} & \cdots & s_{u_{1,n_d}} \\ s_{u_{2,1}} & s_{u_{2,2}} & \cdots & s_{u_{2,n_d}} \\ \vdots & \vdots & \ddots & \vdots \\ s_{u_{n,1}} & s_{u_{n,2}} & \cdots & s_{u_{n,n_d}} \end{bmatrix} = T\left\{ \begin{bmatrix} \xi_{1,1} & \xi_{1,2} & \cdots & \xi_{1,n_d} \\ \xi_{2,1} & \xi_{2,2} & \cdots & \xi_{2,n_d} \\ \vdots & \vdots & \ddots & \vdots \\ \xi_{n,1} & \xi_{n,2} & \cdots & \xi_{n,n_d} \end{bmatrix} \begin{bmatrix} \mathscr{L}_{1,1} & \mathscr{L}_{1,2} & \cdots & \mathscr{L}_{1,n_d} \\ 0 & \mathscr{L}_{2,2} & \cdots & \mathscr{L}_{2,n_d} \\ \vdots & \vdots & \ddots & \vdots \\ 0 & 0 & \cdots & \mathscr{L}_{n_d,n_d} \end{bmatrix} \right\} \tag{15}$$

Subsequently, the likelihood function $L(\boldsymbol{x})$ are subdivided into n_d sub-likelihood functions. The Bayesian model updating of geomaterial parameters using the proposed approach is implemented in a sequential procedure, as shown in Fig. 1. The posterior samples of geomaterial parameters obtained from the current round of updating are treated as the prior samples for the next round of updating. For illustration, the first sub-likelihood function $W_1(\boldsymbol{x})$ can be expressed as

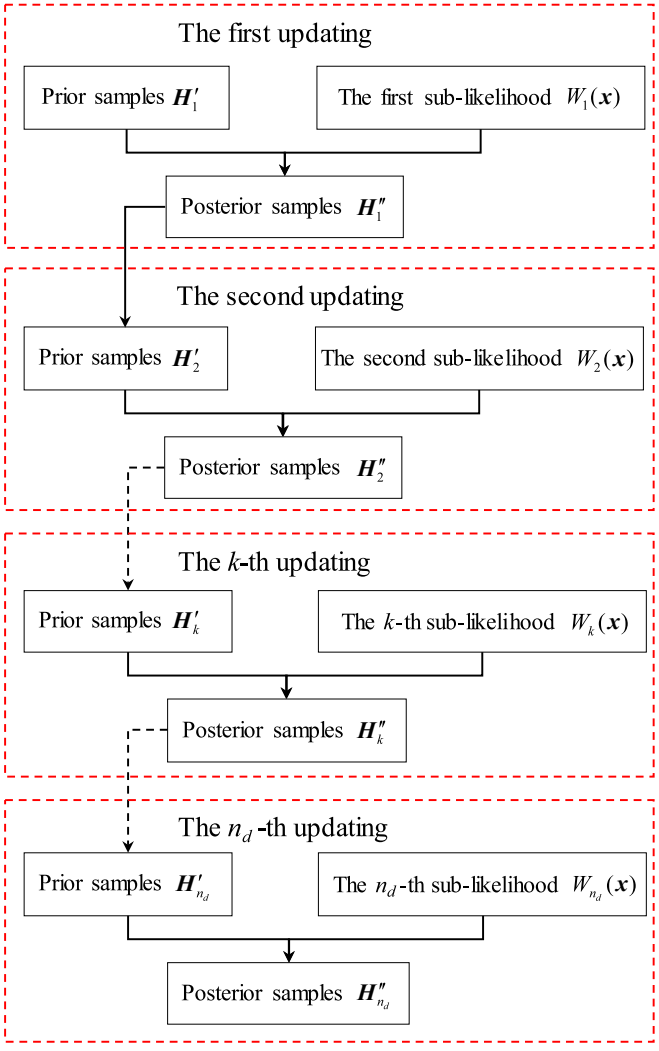

Fig. 1. Schematic illustration of the sequential updating using the proposed method.

$$W_1(\boldsymbol{x}) = \frac{1}{\sqrt{2\pi}\sigma_\varepsilon}\exp\left\{ -\frac{\left[s_{u_1}^m - T(\xi_{j,1}\mathscr{L}_{1,1})\right]^2}{2\sigma_\varepsilon^2} \right\} \tag{16}$$

The corresponding failure domain Ω_{acc}^1 for the first sub-likelihood function is given by

$$\Omega_{acc}^1 = \{g_1(\boldsymbol{x}) = U_1 - c_1 W_1(\boldsymbol{x}) \le 0\} \tag{17}$$

Once the failure domain Ω_{acc}^1 is determined, the subset simulation can be employed to solve the equivalent structural reliability problem with the driving variable $g_1(\boldsymbol{x})$. The probability $P\{g_1(\boldsymbol{x}) \le 0\}$ can be expressed as the product of a series of conditional probabilities of intermediate events with larger probability values. When the random samples reach the failure domain Ω_{acc}^1, the subset simulation terminates. Among the samples falling within Ω_{acc}^1, $n_s = np_0$ samples are then considered as seed samples, where n and p_0 represent, respectively, the number of samples of that level in the subset simulation and the conditional probability.

Then, the improved Metropolis-Hastings algorithm [3] is employed to expand the n_s samples in that level to n samples, labelled as $\boldsymbol{\zeta}_1 = (\zeta_{1,1}, \zeta_{2,1}, \cdots, \zeta_{n,1})^{\mathrm{T}}$. A set of $n \times (l-1)$ standard normal random samples are generated to be combined with $\boldsymbol{\zeta}_1$ to form the prior samples $\boldsymbol{H}_2'$ for the next round of Bayesian model updating:

$$\boldsymbol{H}_2' = T\left\{ \begin{bmatrix} \zeta_{1,1} & \xi_{1,2} & \cdots & \xi_{1,l} \\ \zeta_{2,1} & \xi_{2,2} & \cdots & \xi_{2,l} \\ \vdots & \vdots & \ddots & \vdots \\ \zeta_{n,1} & \xi_{n,2} & \cdots & \xi_{n,l} \end{bmatrix} \begin{bmatrix} \mathscr{L}_{1,1} & \mathscr{L}_{1,2} & \cdots & \mathscr{L}_{1,l} \\ 0 & \mathscr{L}_{2,2} & \cdots & \mathscr{L}_{2,l} \\ \vdots & \vdots & \ddots & \vdots \\ 0 & 0 & \cdots & \mathscr{L}_{l,l} \end{bmatrix} \right\} \tag{18}$$

Comparing Eq. (18) with Eq. (15), it is evident that the first round of Bayesian model updating only updates the first column vector in the original sample matrix space. Similarly, for the second round of Bayesian model updating, the second sub-likelihood function is constructed as follows:

$$W_2(\boldsymbol{x}) = \frac{1}{\sqrt{2\pi}\sigma_\varepsilon}\exp\left\{ -\frac{\left[s_{u_2}^m - T(\zeta_{j,1}\mathscr{L}_{1,2} + \xi_{j,2}\mathscr{L}_{2,2})\right]^2}{2\sigma_\varepsilon^2} \right\} \tag{19}$$

As seen in the above equation, based on the second sub-likelihood function $W_2(\boldsymbol{x})$, the Bayesian model updating only requires updating the second column vector in the original sample matrix space [e.g., $\boldsymbol{\xi}_2 = (\xi_{1,2}, \xi_{2,2}, \cdots, \xi_{n,2})^{\mathrm{T}}$]. As a result, the second sub-likelihood function remains a one-dimensional function, significantly increasing the sample acceptance rate. After obtaining the updated $\boldsymbol{\zeta}_2$ (i.e., expanded from the n_s seed samples) for the second sub-likelihood function, a set of $n \times (l-2)$ standard normal random samples are then generated to be combined with $\boldsymbol{\zeta}_1$ and $\boldsymbol{\zeta}_2$ to form the prior samples $\boldsymbol{H}_3'$ for the third round (i.e., third round) of Bayesian model updating:

$$\boldsymbol{H}_3'(\boldsymbol{x}) = T\left\{ \begin{bmatrix} \zeta_{1,1} & \zeta_{1,2} & \xi_{1,3} & \cdots & \xi_{1,l} \\ \zeta_{2,1} & \zeta_{2,2} & \xi_{2,3} & \cdots & \xi_{2,l} \\ \vdots & \vdots & \vdots & \ddots & \vdots \\ \zeta_{n,1} & \zeta_{n,2} & \xi_{n,3} & \cdots & \xi_{n,l} \end{bmatrix} \begin{bmatrix} \mathscr{L}_{1,1} & \mathscr{L}_{1,2} & \cdots & \mathscr{L}_{1,l} \\ 0 & \mathscr{L}_{2,2} & \cdots & \mathscr{L}_{2,l} \\ \vdots & \vdots & \ddots & \vdots \\ 0 & 0 & \cdots & \mathscr{L}_{l,l} \end{bmatrix} \right\} \tag{20}$$

This process continues iteratively for all n_d samples and sub-likelihood functions, resulting in the final posterior samples of geomaterial parameters as follows:

$$\boldsymbol{H}''_{n_d} = T\left\{ \begin{bmatrix} \zeta_{1,1} & \zeta_{1,2} & \cdots & \zeta_{1,n_d} & \xi_{1,n_d+1} & \cdots & \xi_{1,l} \\ \zeta_{2,1} & \zeta_{2,2} & \cdots & \zeta_{2,n_d} & \xi_{2,n_d+1} & \cdots & \xi_{2,l} \\ \vdots & \vdots & \ddots & \vdots & \vdots & \ddots & \vdots \\ \zeta_{n,1} & \zeta_{n,2} & \cdots & \zeta_{n,n_d} & \xi_{n,n_d+1} & \cdots & \xi_{n,l} \end{bmatrix} \begin{bmatrix} \mathscr{L}_{1,1} & \mathscr{L}_{1,2} & \cdots & \mathscr{L}_{1,l} \\ 0 & \mathscr{L}_{2,2} & \cdots & \mathscr{L}_{2,l} \\ \vdots & \vdots & \ddots & \vdots \\ 0 & 0 & \cdots & \mathscr{L}_{l,l} \end{bmatrix} \right\} \tag{21}$$

It is worth noting that the key step in the improved BUS method is the

employment of the improved Metropolis-Hastings algorithm to expand each set of n_s seed samples obtained from the Bayesian model updating to a larger sample size (i.e., n samples). Fig. 2 further illustrates the improved Metropolis-Hastings algorithm, and a pseudocode of the algorithm is given in Fig. 3. The specific calculation process of the improved Metropolis-Hastings algorithm is summarized as follows:

(i) Treat each set of $n_s = np_0$ samples that fall within the failure domain as a set of seed samples, i.e., $\boldsymbol{\zeta}_k = (\zeta_{1,k}, \zeta_{2,k}, \cdots, \zeta_{n_s,k})^{\mathrm{T}}$. This is shown in Fig. 2(b).

(ii) For the t-th seed sample in $\boldsymbol{\zeta}_k$, i.e., $\zeta_{t,k}$, a uniform distribution

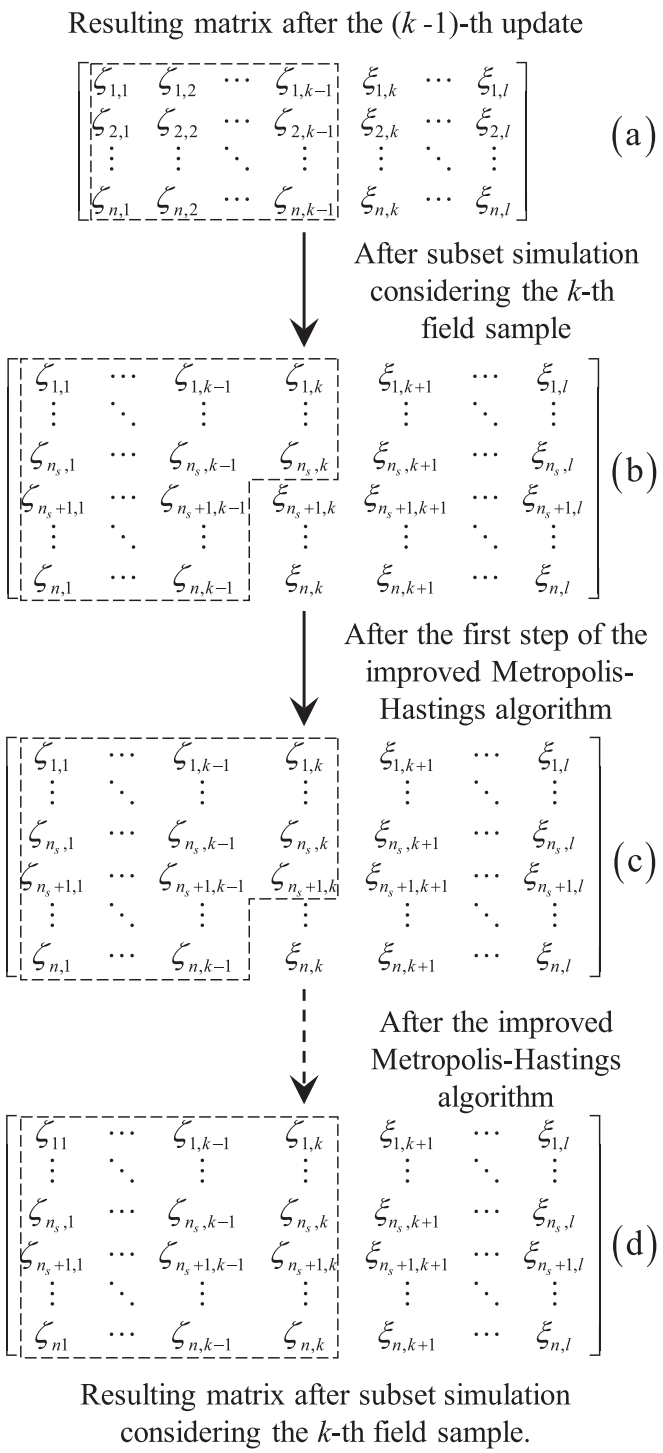

Fig. 2. Illustration of sample augmentation using the improved Metropolis-Hastings algorithm.

with a center at $\zeta_{t,k}$ and a width of 2 is used to generate the m-th additional sample v, where $m = 1, 2, \ldots, n\text{-}n_s$. The following condition is then adopted to accept or reject the generated sample v:

$$\theta = \begin{cases} v, & \text{with prob. } \min\{1, r_t\} \\ \zeta_{t,k}, & \text{with prob. } 1 - \min\{1, r_t\} \end{cases} \tag{22}$$

where $r_t = q(v)/q(\zeta_{t,k})$, and $q(.)$ is the PDF of a standard normal variable (e.g., [32]).

(iii) Concatenate the candidate sample θ with the $(n_s + m)$-th row of additional samples from the first to the (k-1)-th round of Bayesian model updating, i.e., $(\zeta_{n_s+m,1}, \zeta_{n_s+m,2}, \cdots, \zeta_{n_s+m,k-1})$, and a set of l-k random variables generated from a standard normal distribution, i.e., $(\xi_{n_s+m,k+1}, \cdots, \xi_{n_s+m,l})$, to form a new candidate sample set $\boldsymbol{\theta}'$, i.e., $\boldsymbol{\theta}' = (\zeta_{n_s+m,1}, \zeta_{n_s+m,2}, \cdots, \zeta_{n_s+m,k-1}, \theta, \xi_{n_s+m,k+1}, \cdots, \xi_{n_s+m,l})$. An illustration after the first step ($m = 1$) in the improved Metropolis-Hastings algorithm is shown in Fig. 2(c). Numerically simulate this random field realization in the slope model and determine whether this sample is located within the slope failure region Ω_F or not. If the candidate sample set $\boldsymbol{\theta}'$ corresponds to a failure realization, the expanded sample θ is accepted.

$$\zeta_{n_s+m,k} = \theta, \text{ if } \boldsymbol{\theta}' \in \Omega_F \tag{23}$$

(iv) If the candidate sample set $\boldsymbol{\theta}'$ does not corresponds to a failure realization, the expanded sample θ is rejected, and return to step (ii), generating a new sample using the next seed sample (i.e., $t = t + 1$). Repeat this process until the candidate sample set $\boldsymbol{\theta}'$ falls within the slope failure region. Then, repeat the entire process until n samples are obtained, forming the illustration shown in Fig. 2(d).

The division of Ω_{acc} in Eq. (11) keeps the properties of the physical problem, as shown in Appendix A, and the final posterior samples of geomaterial parameters obtained using the Bayesian model updating with n_d field data unconditionally fall within Ω_{acc}, which has also been previously demonstrated by Wang and Shafieezadeh [40]. With these final posterior samples $\boldsymbol{H}'_{n_d}$, the methods such as subset simulation can be further utilized to estimate the posterior failure probability of the slope. Fig. 4 presents the flowchart of the overall implementation procedures of the proposed improved BUS method.

4. Illustrative example

4.1. Model descriptions

To validate the effectiveness of the proposed improved BUS method in the Bayesian model updating of spatially variable geomaterial parameters using a large volume of field data, a comparison with traditional MCMC and original BUS methods is made based on an example involving an undrained saturated soil slope (e.g., [19]).

The model, illustrated in Fig. 5, pertains to a slope with a height of 10 m, a slope ratio of 1:2, and a soil unit weight $\gamma_{sat} = 20$ kN/m^3. The undrained shear strength s_u is assumed to follow a normal distribution with a mean of 40 kPa and a standard deviation of 10 kPa (e.g., [39]). As shown in Fig. 5, a deterministic slope stability analysis using the simplified Bishop method and the mean s_u value (i.e., 40 kPa) is first carried out to obtain a factor of safety (FS) of 1.182, which agrees with the result reported by Wang et al. [39] (i.e., FS=1.178), demonstrating the validity of the numerical model used in the present study.

For the subsequent probabilistic slope stability analyses, a two-dimensional single exponential autocorrelation function is chosen with the horizontal and vertical scales of fluctuation specified as 38 m and 3.8 m, respectively, according to Phoon and Kulhawy [33] and Jiang et al. [19]. The slope domain is discretized into 910 mixed random field elements with a width of 2.0 m and a height of 0.5 m, including both quadrilateral and triangular elements, as shown in Fig. 5. The ratio of the width of the random field element to the horizontal scale of

for $m = 1 : n - n_s$ **do**

% Total ($n - n_s$) samples to be generated

$t = 1$, stop_flag = 0

% Determining seed samples and loop stop flags

While stop_flag == 0 **do**

a. Generate sample υ form a uniform distribution with a center at $\zeta_{t,k}$ and a width of 2

b. Accept or reject υ

$$\theta = \begin{cases} \upsilon, \text{ with prob. } \min\{1, r_t\} \\ \zeta_{t,k}, \text{ with prob. } 1 - \min\{1, r_t\} \end{cases}$$

c. Concatenate the candidate sample θ with the (n_s+m)-th rows of additional samples from the first to the (k-1)-th round of Bayesian model updating, and a set of l-k random samples generated from a standard normal distribution to form a new candidate sample set $\boldsymbol{\theta}'$

$$\boldsymbol{\theta}' = \left(\zeta_{n_s+m,1}, \zeta_{n_s+m,2}, \cdots, \zeta_{n_s+m,k-1}, \theta, \xi_{n_s+m,k+1}, \cdots, \xi_{n_s+m,l}\right)$$

if $\boldsymbol{\theta}' \in \Omega_F$ **then**

% Determine if $\boldsymbol{\theta}'$ is in the failure region Ω_F

$\zeta_{n_s+m,k} = \theta$, stop_flag == 1

Break

end if

if $t == n_s$ **then**

% Changing seed samples

$t = 1$

else

$t = t + 1$

end if

end while

end for

Fig. 3. Pseudocode of sample augmentation using the improved Metropolis-Hastings algorithm.

fluctuation is 0.053, while the ratio of the height of the random field element to the vertical scale of fluctuation is 0.132. As demonstrated by Der Kiureghian and Ke [8] that an accurate representation of a random field can be achieved when the element size is less than 0.25 of the scale of fluctuation for the exponential autocorrelation function. In this regard, the proposed random field discretization scheme is sufficient to provide an accurate representation of the random field of s_u and a reliable estimate of the probability of slope failure. Based on this configuration and the prior statistics of s_u, stationary normal random field realizations of s_u are generated using the Cholesky decomposition-based midpoint method. A Monte Carlo simulation (MCS) involving 100,000 realizations is then employed to assess the probability of slope failure using the limit state function of $G(\boldsymbol{x}) = FS(\boldsymbol{x}) - 1.0$, and the obtained result is 19.45 %.

4.2. Test case 1

As shown in Figs. 5 and 6, field vane shear tests (VST) are performed on the borehole BH1 and provide $n_d = 14$ sets of undrained shear strength data (e.g., [2]). Two representative locations, A ($x = 23$ m, $z = -7.75$ m) and B ($x = 23$ m, $z = -19.25$ m) within the slope region are then chosen to illustrate the results of Bayesian model updating.

Using the 14 sets of s_u data and Eq. (12), sub-likelihood functions are constructed based on a standard deviation of measurement error of $\sigma_\varepsilon = 2.0$ kPa. Note that $\sigma_\varepsilon = 2.0$ kPa is adopted according to the literature (e.g., [19,30]) and used for both the original BUS and the improved BUS methods. Coupled with the improved Metropolis-Hastings algorithm, the proposed improved BUS method is implemented to calculate the posterior distribution of s_u. Specifically, $n = 500$ and $p_0 = 0.1$ are chosen for implementing the improved BUS method. In addition, for comparison, the traditional MCMC method and the original BUS method (i.e., $n = 1000$ and $n = 50{,}000$ and $p_0 = 0.1$) are also implemented using the same field data. It is worth noting that the analyses using all the three methods are repeated 10 times to obtain 10 sets of independent results for comparing the consistency and robustness of the methods.

Table 1 presents the information about the 14 sub-likelihood functions, including the number of simulation levels and the average sample acceptance rate for each sub-likelihood function. Compared to the original BUS method, which requires five subset simulation levels to obtain samples in the failure region of the high-dimensional likelihood function, the proposed improved BUS method only needs at most three subset simulation levels for each sub-likelihood function. In addition, the sample acceptance rates for all sub-likelihood functions in the proposed improved BUS method are much higher than that for the original

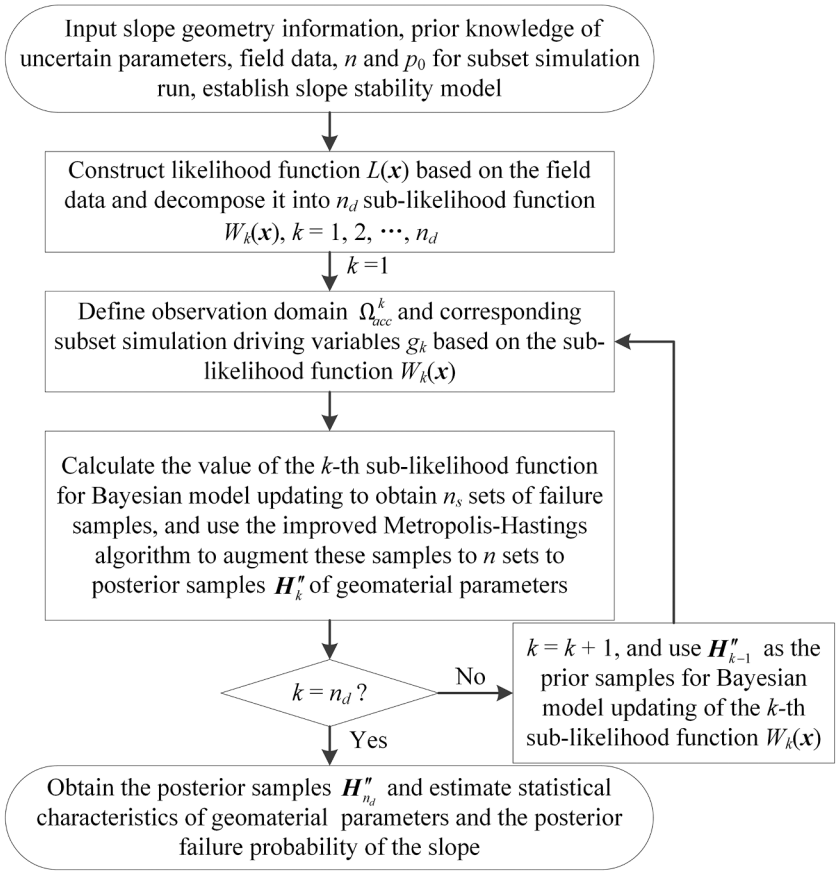

Fig. 4. Flowchart for the implementation of the proposed method.

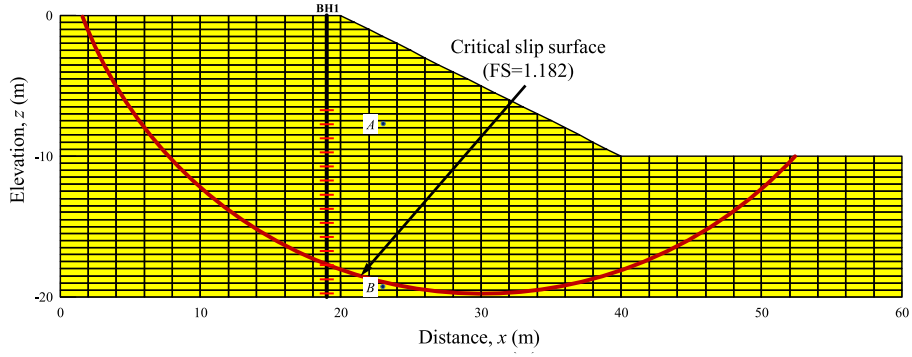

Fig. 5. Slope model and results of a deterministic stability analysis.

BUS method (i.e., 3.2×10^{-5}). In this case, the proposed improved BUS method takes only 74 s to perform 10 independent undrained shear strength updates on a desktop computer with 32 GB of memory and Intel i5-14600 processor clocked at 3.5 GHz. In contrast, the original BUS method with $n = 1000$ takes 358 s using the same computer. These results indicate that the improved BUS method, by subdividing the likelihood function into multiple sub-likelihood functions, significantly improves the sample acceptance rate, which in turn reduces the computational burden of the Bayesian model updating involving high-dimensional data. Fig. 7(a) and (b) present, respectively, the posterior PDFs of s_u at locations A and B obtained from the 10 independent calculations and the average results using the improved BUS method. The posterior PDFs estimated from the averages of all posterior samples of s_u are treated as the final results.

Figs. 8(a) and (b) provide, respectively, a comparison of the posterior PDFs of s_u at locations A and B obtained using the three methods. The corresponding prior distribution is also included in the figures for comparison. The figures show that, in comparison to the prior distribution, the posterior distributions obtained by the various methods are taller and narrower, indicating that the standard deviation noticeably decreases. It is also noted that the means of the posterior distributions also approach the values of field VST data at the corresponding depths. However, the posterior distributions of s_u at locations A and B obtained using the original BUS method ($n = 1000$) exhibit multiple peaks. This observation is attributed to the extremely low sample acceptance rate (i.e., 3.2×10^{-5}) resulted from the small value of the likelihood function constructed based on the 14 sets of s_u field data, thereby undermining the stability of the original BUS method. While the number of samples for each simulation level is increased to 50,000 ($n = 50{,}000$) for the original BUS method, the estimated posterior PDFs at locations A and B

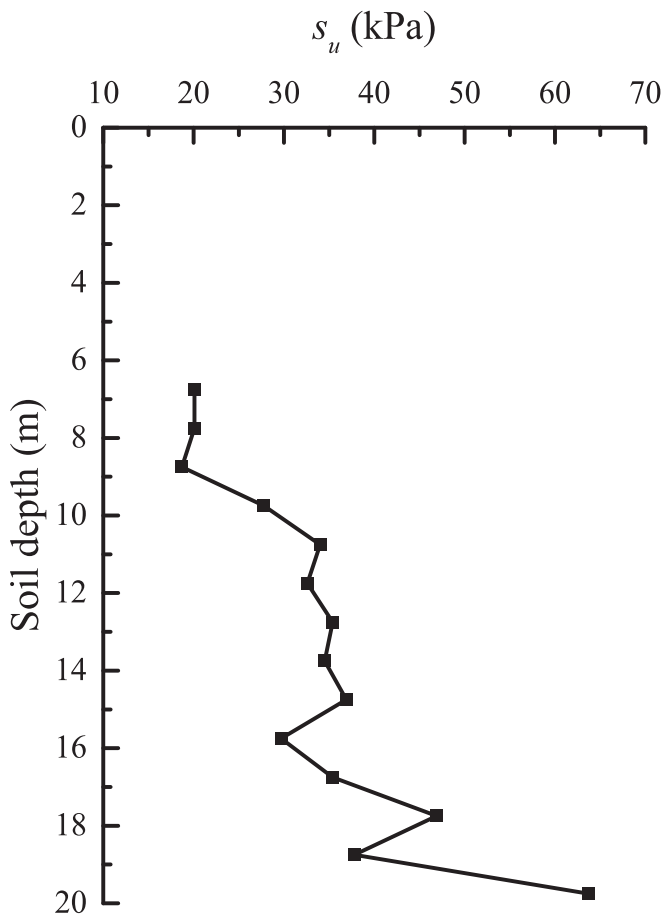

Fig. 6. 14 undrained shear strength data obtained from field vane shear tests (e.g., [2]).

become smoother and match better with the results of the proposed method. Although a small volume ($n_d = 14$) of field data is incorporated in this case, a very large augmented sample size is required for the original BUS method to obtain results with reasonable accuracy, which undoubtedly imposes a significant computational burden.

As illustrated in Fig. 8, in comparison with those obtained from the original BUS method. The proposed improved BUS method, which always updates one-dimensional variables in each sub-likelihood function, achieves a higher sample acceptance rate, leading to smoother posterior distributions at both locations *A* and *B*. The results also better match with those obtained using the brute-force MCMC method. It is evident that the proposed improved BUS method can effectively integrate a large volume of field data for efficient Bayesian model updating of spatially varying geomaterial parameters. In addition, the tails of the posterior PDFs of s_u at both locations *A* and *B* differ between the MCMC method and the proposed method. This is because the classic MCMC method is prone to slow convergence, especially in the tails of the distribution where the probabilities are low in such a high-dimensional Bayesian model updating problem [19]. These differences further demonstrate that the proposed method effectively overcomes the limitations of the classic MCMC method.

4.3. Test case 2

Clearly, a single borehole, BH1, with 14 sets of s_u field data adopted in test case 1 is not sufficient for the Bayesian model updating of a complex problem. This motivates the consideration of test case 2 wherein multiple boreholes with massive field data are incorporated into the Bayesian model updating of spatially variable undrained shear strength over a larger area. In test case 2, eight additional boreholes (i.e., BH2 to BH9) are introduced to the slope model, as shown in Fig. 9. Such a large volume of field data can also be used to further validate the effectiveness of the improved BUS method. Fig. 9 provides details regarding a reference conditional random field realization and planning of the nine boreholes. The 110 sets of undrained shear strength data associated with the nine boreholes are selected from a conditional random field realization generated based on the 14 sets of s_u data of BH1. The procedure of generating the undrained shear strength data corresponding to the eight additional boreholes is summarized as follows:

(1) Adopt the Cholesky decomposition-based midpoint method to discretize the random field of s_u and perform Bayesian model updating to produce posterior random field realizations of s_u conditioned to the 14 sets of s_u data of BH1.

(2) Select one typical posterior random field realization as the reference conditional random field realization (see Fig. 9), determine the eight additional borehole locations and the corresponding sampling locations in the slope, and then extract the values of s_u at the 110 sampling locations associated with the nine boreholes from the reference conditional random field realization as the undrained shear strength data, as shown in Fig. 10.

The likelihood function value constructed directly using the 110 sets of s_u data from the nine boreholes is extremely small, on the order of 10^{-1261}, which is significantly below the precision of computer floating-point operations. This situation could make the Bayesian model updating of geomaterial parameters and slope reliability assessment computationally expensive and inaccurate, further justifying the need for an improved method to address this technical challenge.

In this test case, in addition to the 110 s_u data, field observations regarding the slope's state, such as FS=a specific value, FS>1.0 or $FS \leq 1.0$, can also be considered in the Bayesian model updating to further learn the distribution of geomaterial parameters. Here, $FS = FS_r$ is regarded as an important piece of field information for the Bayesian model updating to further demonstrate the effectiveness of the proposed improved BUS method. FS_r is the factor of safety calculated based on the reference random field realization in the slope stability analysis, corresponding to the conditional random field used to generate the data of eight additional boreholes. A model bias, η, is then introduced to characterize model uncertainty in the slope stability analysis, which is defined as the difference between the actual factor of safety, FS_r, and model-predicted factor of safety, $FS(\boldsymbol{x})$:

Table 1
Number of subset simulation levels and average sample acceptance rate corresponding to each sub-likelihood function.

Number of Sub-likelihood functions	Subset simulation levels	Sample acceptance rate	Number of Sub-likelihood functions	Subset simulation levels	Sample acceptance rate
1	2	0.0303	8	1	0.222
2	1	0.1616	9	1	0.233
3	1	0.1167	10	1	0.1474
4	1	0.2408	11	1	0.2396
5	1	0.2338	12	1	0.1339
6	1	0.2266	13	1	0.1784
7	1	0.2428	14	3	0.0072

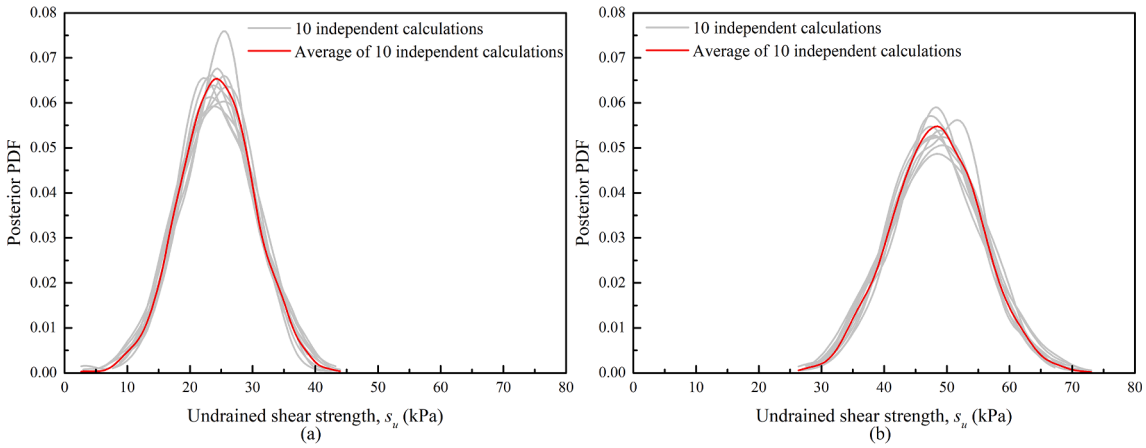

Fig. 7. Comparison of the posterior PDFs of undrained shear strength estimated from 10 independent computations and the average results using the proposed method: (a) location *A*; (b) location *B*.

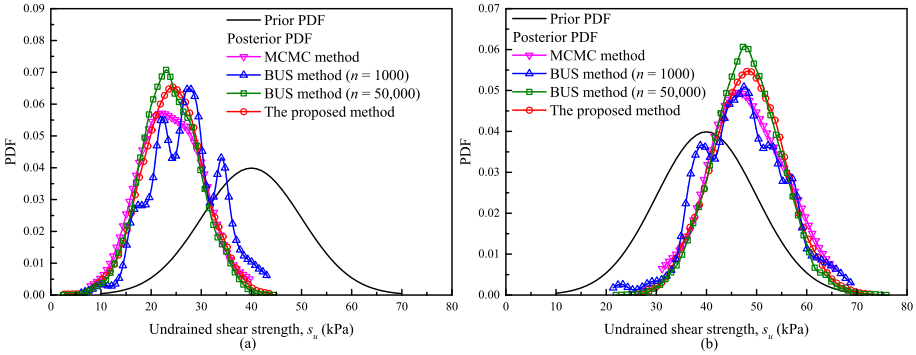

Fig. 8. Comparison of the PDFs of undrained shear strengths at the two representative locations inferred using different methods: (a) location *A*; (b) location *B*.

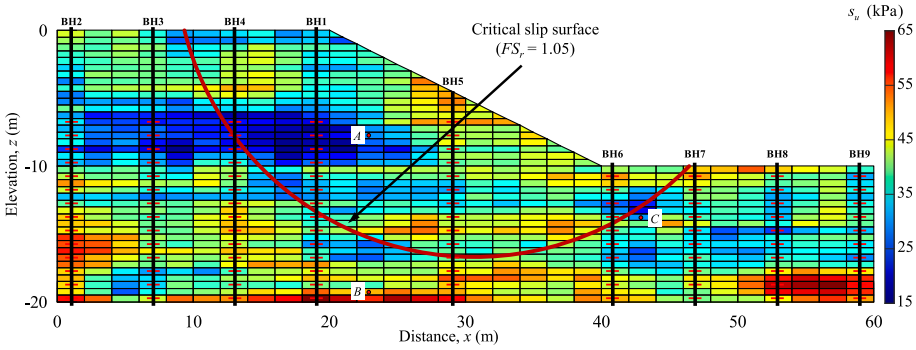

Fig. 9. Reference conditional random field realization and planning of borehole locations.

$$FS_r = FS(\boldsymbol{x}) + \eta \tag{24}$$

Based on the reference random field realization shown in Fig. 9, $FS_r = 1.05$ is obtained in this test case. Assuming that η follows a normal distribution (e.g., [39,38,19,27], the likelihood function that integrates information from the actual factor of safety of the slope is presented as follows:

$$L^o(\boldsymbol{x}) = \phi\left(\frac{FS(\boldsymbol{x}) + \mu_\eta - FS_r}{\sigma_\eta}\right) \tag{25}$$

where $\phi(\cdot)$ represents the standard normal PDF; μ_η and σ_η are the mean and standard deviation of η, respectively. Based on the literature (e.g., [6,44]), $\mu_\eta = 0$ and $\sigma_\eta = 0.05$.

Similar to test case 1, $n = 500$ and $p_0 = 0.1$ are chosen for implementing the improved BUS method while $n = 50{,}000$ and $p_0 = 0.1$ are chosen for implementing the original BUS method. To ensure the robustness in the computational results, both methods are also repeated 10 times, and the average of the 10 independent sets are taken as the final results. Additionally, the Hoffman method (e. g., [15,13,18]), a conditional random field simulation method, is employed here to provide reference posterior distribution and probability of failure for comparison. The Hoffman method can give exact posterior predictions of geomaterial parameters at measurement locations and estimate the posterior values at other locations through the autocorrelation structure between these locations. In addition to locations *A* and *B*, a third location *C* (x = 43 m, z = −13.75 m) is also chosen for illustrations (see Fig. 9).

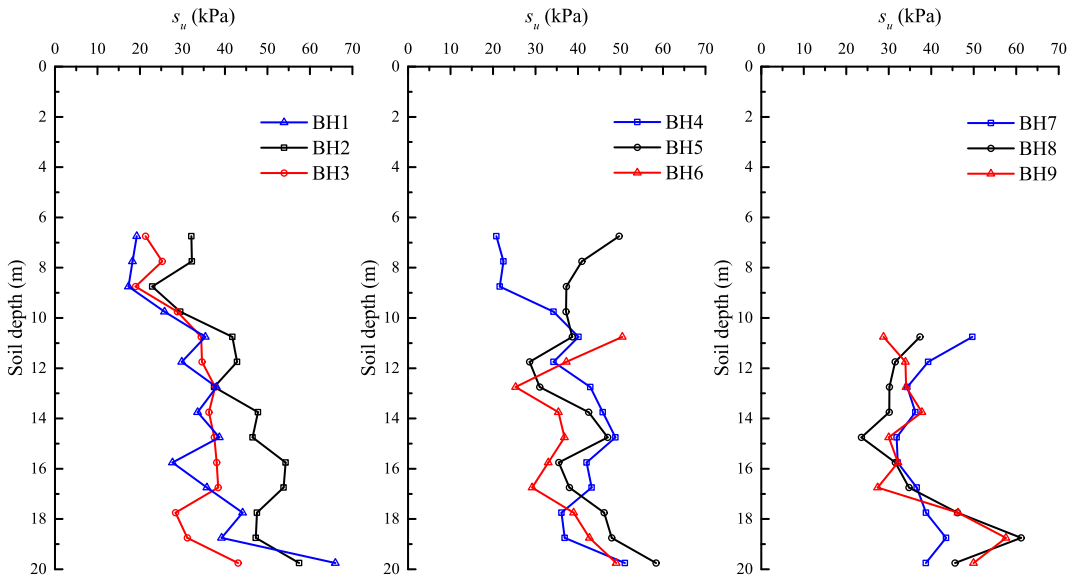

Fig. 10. 110 simulated undrained shear strength data obtained from the nine boreholes.

Fig. 11 compares the posterior PDFs of s_u at locations *A, B* and *C* obtained using different methods. The comparisons also include (i) the integration of only 110 s_u data, and (ii) the integration of both the 110 s_u data and the factor of safety of the slope ($FS_r = 1.05$). It is evident in Fig. 11 that when employing the original BUS method to integrate a substantial amount of field data, the resulting posterior distributions are not sufficiently smooth and exhibit multiple peaks with noticeable discrepancies from the results of the proposed method even though a very large sample size $n = 50{,}000$ for each subset simulation level is used. This issue is attributed to the original BUS method's handling of the high-dimensional likelihood function, which involves repeated applications of the improved Metropolis-Hastings algorithm for sample augmentation (e.g., [34]). This process generates numerous redundant samples, resulting in a very low sample acceptance rate (on the order of 10^{-24}) and quality deterioration in the posterior samples, particularly for cases that incorporate a substantial volume of field data (e.g., [22]). Approximately 24 subset simulation levels are then required to reach the failure region. Unlike test case 1, increasing the sample size is inadequate to overcome the challenge posed by the low acceptance rate of the original BUS method. In contrast, the proposed improved BUS method reduces the generation of redundant samples, achieving a higher sample acceptance rate. Consequently, the inferred posterior distributions are much smoother. In addition, the posterior PDFs of s_u at the three representative locations and the posterior PDFs of *FS* (see Fig. 12) of the proposed method are consistent with those obtained from the Hoffman method when 110 s_u data is incorporated. This further confirms the effectiveness of the proposed method.

In addition to the posterior distributions of s_u, a comparison involving the posterior PDFs of the factor of safety inferred using different methods is presented in Fig. 12. Similar to Fig. 11, the comparisons also include the integration of only 110 s_u data, and the integration of both the 110 s_u data and the factor of safety ($FS_r = 1.05$). It is evident in Fig. 12 that compared to the original BUS method, the posterior PDFs of the factor of safety inferred using the proposed improved BUS method are much smoother. Furthermore, the posterior PDF of the factor of safety inferred using the proposed method with only 110 s_u data is in good agreement with that from the Hoffman method. This confirms that the improved BUS method can effectively handle multiple types of field data in the Bayesian model updating of geomaterial parameters. Most importantly, the results highlight that the improved BUS method can also effectively interpret the information provided by the individual field data although the field s_u data is much larger than the field observation data in quantity in this test case.

Table 2 further compares the posterior means and standard deviations of s_u at locations *A*, *B* and *C*, as well as the posterior probability of slope failure obtained using different methods and different field data. According to Table 2, the posterior statistics (i.e., mean and standard deviation) of s_u and the posterior probability of failure obtained from the improved BUS method are in good agreement with the results of the Hoffman method. Moreover, the posterior means associated with the improved BUS method at the three locations agree better with the benchmark values obtained from the reference conditional random field realization as shown in Fig. 9 (i.e., $s_u = 27.47$ kPa at location *A*, $s_u = 49$ kPa at location *B* and $s_u = 31.37$ kPa at location *C*). It is also observed that the posterior standard deviations and posterior probabilities of failure associated with the improved BUS method are smaller than the results of the original BUS method, indicating that the additional information embedded in the field data can be more effectively extracted by the improved BUS method. In addition, when using the original BUS method with only the 110 s_u data, the calculated probability of slope failure is 0.35, significantly higher than the 0.29 obtained using the proposed improved BUS method and the Hoffman method, suggesting that the slope reliability assessment results obtained by the original BUS method are considerably more conservative. Such a conservativeness in the original BUS method may lead to unnecessary resources utilized for risk mitigation and reinforcement design of the slope.

To further demonstrate the accuracy of the proposed improved BUS method in conducting the Bayesian model updating of spatially variable geomaterial parameters, Fig. 13 compares the posterior means and standard deviations of random field realizations obtained using different methods when integrating different types of field data. Note that the posterior mean and standard deviation of s_u for each random field element shown in Fig. 13 are evaluated by averaging across all the posterior samples obtained from 10 independent calculations via a conventional statistical analysis. The reference conditional random field realization is shown in Fig. 9. By a visual inspection, it is observed that the posterior mean random field realizations calculated using the proposed improved BUS method [i.e., Fig. 13(e) and (i)] reasonably agree with the reference random field realization and that calculated using the Hoffman method [i.e., Fig. 13(c)], whereas the posterior mean random field realizations computed by the original BUS method [i.e., Fig. 13(a) and (g)] are in a large discrepancy with the reference random field realization and that calculated using the Hoffman method. In addition, the posterior standard deviations calculated by the original BUS method

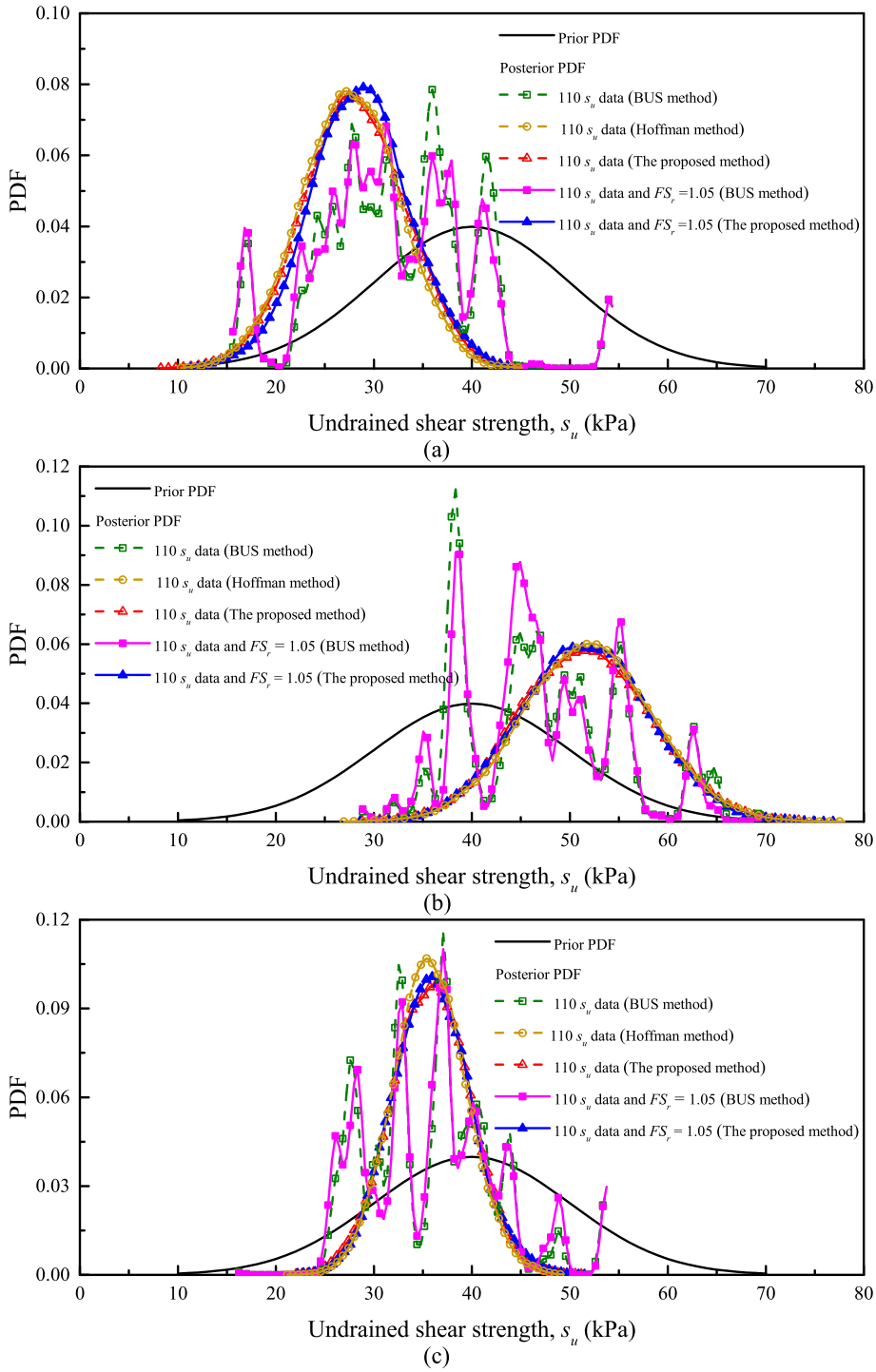

Fig. 11. Comparison of the PDFs of undrained shear strengths at the three representative locations inferred using different methods: (a) location *A*; (b) location *B*; (c) location *C*.

[i.e., Fig. 13(b) and (h)] are significantly larger than those calculated by the improved BUS method [i.e., Fig. 13(f) and (j)] and the Hoffman method [i.e., Fig. 13(d)], especially at the locations of the boreholes and their neighboring soils. This provides additional evidence to support the effectiveness of the improved BUS method.

Fig. 14 compares the posterior means of s_u calculated by different methods for all the 910 random field elements with the corresponding s_u values of reference conditional random field. Scatters closer to the 1:1 line indicates that the posterior mean distribution of s_u is closer to the reference values. It is seen that the coefficient of determination (R^2) for the posterior means calculated using the original BUS method with only the 110 s_u data is only 0.54, which is much smaller than the corresponding R^2 (0.69 and 0.72) by the improved BUS method and Hoffman method, respectively. This indicates that compared with the original BUS method, the correlation between the calculated results and the reference values is higher and the Bayesian model updating results are more reliable when using the proposed improved BUS method. When integrating both the 110 s_u data and the factor of safety information, the R^2 calculated by the proposed improved BUS method obtains a slight increase. For example, the R^2 of the proposed improved BUS method is

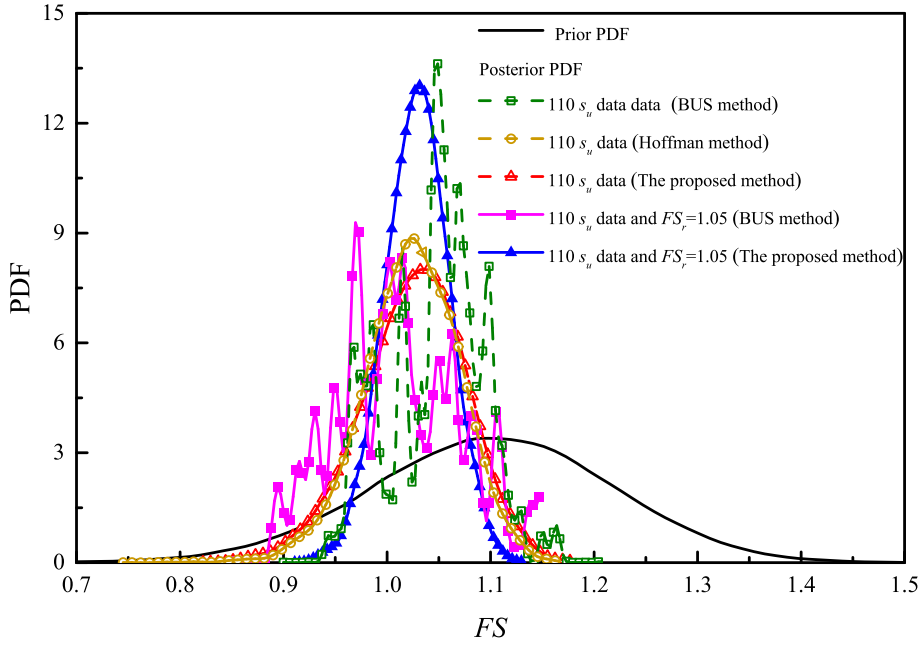

Fig. 12. Comparison of the PDFs of factor of safety inferred using different methods.

further increased to 0.70. This indicates that the closer the generated posterior random field of s_u is to the reference random field when the more field information is integrated.

In addition, to illustrate the accuracy and stability of the posterior probabilities of slope failure calculated by the proposed method, Table 3 compares the statistical parameters of posterior probabilities of slope failure calculated using 10 independent subset simulations between the proposed method and the original BUS method. It can be seen that the variability of the posterior probability of slope failure calculated by the proposed method is less than that calculated by the original BUS method. For example, when only the borehole data are considered, the range $\left(R_{p_f}\right)$ and coefficient of variation $\left(COV_{p_f}\right)$ calculated by the original BUS method are 0.66 and 0.69, respectively, which are much larger than the range and coefficient of variation calculated by the proposed method, which are 0.07 and 0.07, respectively. This is due to the fact that the posterior distribution computed by the original BUS method has a large number of repetitive samples, and these repetitive samples significantly affect the accuracy and consistency of the subsequent estimated probability of slope failure, while the proposed improved BUS method reduces the generation of repetitive samples; therefore, the computed probability of failure is more robust and consistent in the repeated runs.

5. Discussions

5.1. Bayesian updating involving correlation structure

It is worth noting that the illustrative examples presented above implicitly assume that all measurement errors (ε) are independent of each other. In reality, this assumption may be valid for measurements taken from different boreholes or different batches of laboratory experiments. However, the measurement errors associated with data surveyed in the same borehole or batch of laboratory tests are likely to be correlated. In this section, a discussion on the applicability of the proposed improved BUS method to data involving correlation is presented. The implementation procedures are similarly explained using the s_u data as the example.

When the correlation between measurement errors exists, the likelihood function can be constructed as follows:

$$
\begin{aligned}
L(\boldsymbol{x}) = \; & \alpha \exp\left[-\frac{1}{2}\left(\boldsymbol{s}_u^m - \boldsymbol{s}_u\right)^{\mathrm{T}} \boldsymbol{\Sigma}^{-1} \left(\boldsymbol{s}_u^m - \boldsymbol{s}_u\right)\right] \\
= \; & \alpha \exp\left\{-\frac{1}{2}\begin{bmatrix} s_{u_1}^m - s_{u_{j,h(1)}} \\ \vdots \\ s_{u_{n_d}}^m - s_{u_{j,h(n_d)}} \end{bmatrix}^{\mathrm{T}} \begin{bmatrix} \sigma_\varepsilon^2 & \sigma_\varepsilon^2\rho_{1,2} & \cdots & \sigma_\varepsilon^2\rho_{1,n_d} \\ \sigma_\varepsilon^2\rho_{2,1} & \sigma_\varepsilon^2 & \cdots & \sigma_\varepsilon^2\rho_{2,n_d} \\ \vdots & \vdots & \ddots & \vdots \\ \sigma_\varepsilon^2\rho_{n_d,1} & \sigma_\varepsilon^2\rho_{n_d,2} & \cdots & \sigma_\varepsilon^2 \end{bmatrix}^{-1} \begin{bmatrix} s_{u_1}^m - s_{u_{j,h(1)}} \\ \vdots \\ s_{u_{n_d}}^m - s_{u_{j,h(n_d)}} \end{bmatrix}\right\}
\end{aligned} \tag{26}
$$

where α is a proportionality constant, $\alpha = \left[(2\pi)^{\frac{n_d}{2}}|\boldsymbol{\Sigma}|^{\frac{1}{2}}\right]^{-1}$;$\boldsymbol{\Sigma}$ is the covariance matrix with a dimension of $n_d \times n_d$, with variances σ_ε^2 in the diagonal cells and covariances $\sigma_\varepsilon^2\rho_{i,j}$ in the off-diagonal cells; $\rho_{i,j}$ is the correlation coefficient between ε_i and ε_j, $i, j = 1, 2, \cdots, n_d$; $\boldsymbol{\Sigma}^{-1}$ is the inversion matrix of $\boldsymbol{\Sigma}$.

Since the likelihood function in this case can no longer be calculated

Table 2
Comparison of the posterior means, standard deviations of undrained shear strength and the probabilities of slope failure obtained from different methods.

Data	Method	Posterior mean (kPa)			Posterior standard deviation (kPa)			Posterior probability of failure
		A	*B*	*C*	*A*	*B*	*C*	
110 s_u data	BUS method	32.35	47.18	36.03	7.73	8.12	6.60	0.35
	Hoffman method	27.61	51.83	35.71	4.99	6.61	3.72	0.29
	The proposed method	27.99	51.50	35.84	5.15	6.72	3.98	0.29
110 s_u data and $FS_r = 1.05$	BUS method	31.74	46.80	36.32	7.86	7.54	6.88	0.19
	The proposed method	28.50	51.50	35.93	4.98	6.50	3.97	0.13

following the rule of multiplication, such as that shown in Eq. (8), it cannot be simply decomposed into several independent sub-likelihood functions as in Eq. (9). Therefore, the following workaround is proposed and validated to deal with the case involving correlated likelihood. The procedures are summarized as follows:

(i) The first individual sub-likelihood function is constructed using a single s_u data following Eq. (27). This is identical to the first step explained in Section 3.2.

$$\begin{aligned} W_1(\boldsymbol{x}) &= \alpha_1 \exp\left\{ -\frac{1}{2}\left[s_{u_1}^m - s_{u_{j,h(1)}}\right]^{\mathrm{T}} \left[\sigma_\varepsilon^2\right]^{-1} \left[s_{u_1}^m - s_{u_{j,h(1)}}\right] \right\} \\ &= \frac{1}{\sqrt{2\pi}\sigma_\varepsilon} \exp\left\{ -\frac{\left[s_{u_1}^m - T(\xi_{j,1}\mathscr{L}_{1,1})\right]^2}{2\sigma_\varepsilon^2} \right\} \end{aligned} \tag{27}$$

(ii) Following Eq. (27) and the procedures explained in Section 3.2, seed samples can be obtained after the first round of Bayesian model updating. The improved Metropolis-Hastings algorithm can then be implemented to expand the seed samples, forming the posterior samples $\boldsymbol{H}'_1$, which is also the prior samples $\boldsymbol{H}'_2$ for the second round of Bayesian model updating as follows. Note that Eq. (28) is also identical to Eq. (18) in Section 3.2.

$$\boldsymbol{H}'_2 = T\left\{ \begin{bmatrix} \zeta_{1,1} & \xi_{1,2} & \cdots & \xi_{1,l} \\ \zeta_{2,1} & \xi_{2,2} & \cdots & \xi_{2,l} \\ \vdots & \vdots & \ddots & \vdots \\ \zeta_{n,1} & \xi_{n,2} & \cdots & \xi_{n,l} \end{bmatrix} \begin{bmatrix} \mathscr{L}_{1,1} & \mathscr{L}_{1,2} & \cdots & \mathscr{L}_{1,l} \\ 0 & \mathscr{L}_{2,2} & \cdots & \mathscr{L}_{2,l} \\ \vdots & \vdots & \ddots & \vdots \\ 0 & 0 & \cdots & \mathscr{L}_{l,l} \end{bmatrix} \right\} \tag{28}$$

(iii) Different from the case considered in Section 3.2, when the second measurement data is included in the Bayesian model updating, there exists a correlation between ε_1 and ε_2. Therefore, the second sub-likelihood function, considering both the first and second measurement data, is constructed as follows:

$$\begin{aligned} W_2(\boldsymbol{x}) &= \alpha_2 \exp\left\{ \begin{bmatrix} s_{u_1}^m - s_{u_{j,h(1)}} \\ s_{u_2}^m - s_{u_{j,h(2)}} \end{bmatrix}^{\mathrm{T}} \boldsymbol{\Sigma}_2^{-1} \begin{bmatrix} s_{u_1}^m - s_{u_{j,h(1)}} \\ s_{u_2}^m - s_{u_{j,h(2)}} \end{bmatrix} \right\} \\ &= \alpha_2 \exp\left\{ -\frac{1}{2} \begin{bmatrix} s_{u_1}^m - T(\zeta_{j,1}\mathscr{L}_{1,1}) \\ s_{u_2}^m - T(\zeta_{j,1}\mathscr{L}_{1,2} + \xi_{j,2}\mathscr{L}_{2,2}) \end{bmatrix}^{\mathrm{T}} \begin{bmatrix} \sigma_\varepsilon^2 & \sigma_\varepsilon^2\rho_{1,2} \\ \sigma_\varepsilon^2\rho_{2,1} & \sigma_\varepsilon^2 \end{bmatrix}^{-1} \begin{bmatrix} s_{u_1}^m - T(\zeta_{j,1}\mathscr{L}_{1,1}) \\ s_{u_2}^m - T(\zeta_{j,1}\mathscr{L}_{1,2} + \xi_{j,2}\mathscr{L}_{2,2}) \end{bmatrix} \right\} \end{aligned} \tag{29}$$

In contrast to Eq. (19) where only the second measurement data is utilized to construct the second sub-likelihood function, Eq. (29) re-utilizes the first measurement data due to the presence of the correlation structure. However, as can be seen in Eq. (29), the results obtained from the previous round of Bayesian model updating, e.g., $\left(\zeta_{1,1}, \zeta_{2,1}, \zeta_{3,1}, \cdots, \zeta_{n,1}\right)^{\mathrm{T}}$, remain unchanged in the second round of Bayesian model updating. This means that the second round of Bayesian model updating only requires updating of the second column vector in the original sample matrix space while considering the correlation structure. The resulting $\boldsymbol{H}'_2$, which is also $\boldsymbol{H}'_3$, will then be used for the third round of Bayesian model updating. Similarly, in calculating the third sub-likelihood function, all first, second and third measurement data are considered in conjunction with their correlation structure. The results obtained in the previous round of updating, e.g., $\left(\zeta_{1,1}, \zeta_{2,1}, \zeta_{3,1}, \cdots, \zeta_{n,1}\right)^{\mathrm{T}}$ and $\left(\zeta_{1,2}, \zeta_{2,2}, \zeta_{3,2}, \cdots, \zeta_{n,2}\right)^{\mathrm{T}}$, remain unchanged. This means that only the third column vector in the original matrix space is updated.

(iv) The procedures described above are then repeated until all n_d sets of s_u data is considered in the Bayesian model updating, and the last sub-likelihood function is expressed as follows:

$$\begin{aligned} W_{n_d}(\boldsymbol{x}) &= \alpha_{n_d} \exp\left[-\frac{1}{2}\left(\boldsymbol{s}_u^m - \boldsymbol{s}_u\right)^{\mathrm{T}} \boldsymbol{\Sigma}_{n_d}^{-1} \left(\boldsymbol{s}_u^m - \boldsymbol{s}_u\right) \right] \\ &= \alpha_{n_d} \exp\left[-\frac{1}{2}\left(\boldsymbol{s}_u^m - \boldsymbol{s}_u\right)^{\mathrm{T}} \begin{bmatrix} \sigma_\varepsilon^2 & \cdots & \sigma_\varepsilon^2\rho_{1,n_d} \\ \vdots & \ddots & \vdots \\ \sigma_\varepsilon^2\rho_{n_d,1} & \cdots & \sigma_\varepsilon^2 \end{bmatrix}^{-1} \left(\boldsymbol{s}_u^m - \boldsymbol{s}_u\right) \right] \end{aligned} \tag{30}$$

$$\begin{aligned} \boldsymbol{s}_u^m - \boldsymbol{s}_u &= \begin{bmatrix} s_{u_1}^m - s_{u_{j,h(1)}} \\ \vdots \\ s_{u_{n_d}}^m - s_{u_{j,h(n_d)}} \end{bmatrix} \\ &= \begin{bmatrix} s_{u_1}^m - T(\zeta_{j,1}\mathscr{L}_{1,1}) \\ \vdots \\ s_{u_{n_d}}^m - T\left(\zeta_{j,1}\mathscr{L}_{1,n_d} + \zeta_{j,2}\mathscr{L}_{2,n_d} \cdots + \zeta_{j,n_d-1}\mathscr{L}_{n_d-1,n_d} + \xi_{j,n_d}\mathscr{L}_{n_d,n_d}\right) \end{bmatrix} \end{aligned} \tag{31}$$

As can be seen in Eqs. (30) and (31), all measurement data have been incorporated in the updating with the complete correlation matrix considered. However, only the last column in the original matrix space, i.e., $\left(\xi_{1,l}, \xi_{2,l}, \xi_{3,l}, \cdots, \xi_{n,l}\right)^{\mathrm{T}}$, is updated while $\left(\zeta_{1,1}, \zeta_{2,1}, \zeta_{3,1}, \cdots, \zeta_{n,1}\right)^{\mathrm{T}}$, $\left(\zeta_{1,2}, \zeta_{2,2}, \zeta_{3,2}, \cdots, \zeta_{n,2}\right)^{\mathrm{T}}$, ..., $\left(\zeta_{1,l-1}, \zeta_{2,l-1}, \zeta_{3,l-1}, \cdots, \zeta_{n,l-1}\right)^{\mathrm{T}}$ remain the same as the results obtained from the previous rounds of Bayesian model updating, effectively avoiding the issue of "curse of dimensionality".

In order to demonstrate the proposed workaround for cases involving correlated measurements, a validation study using the same 14 sets of s_u

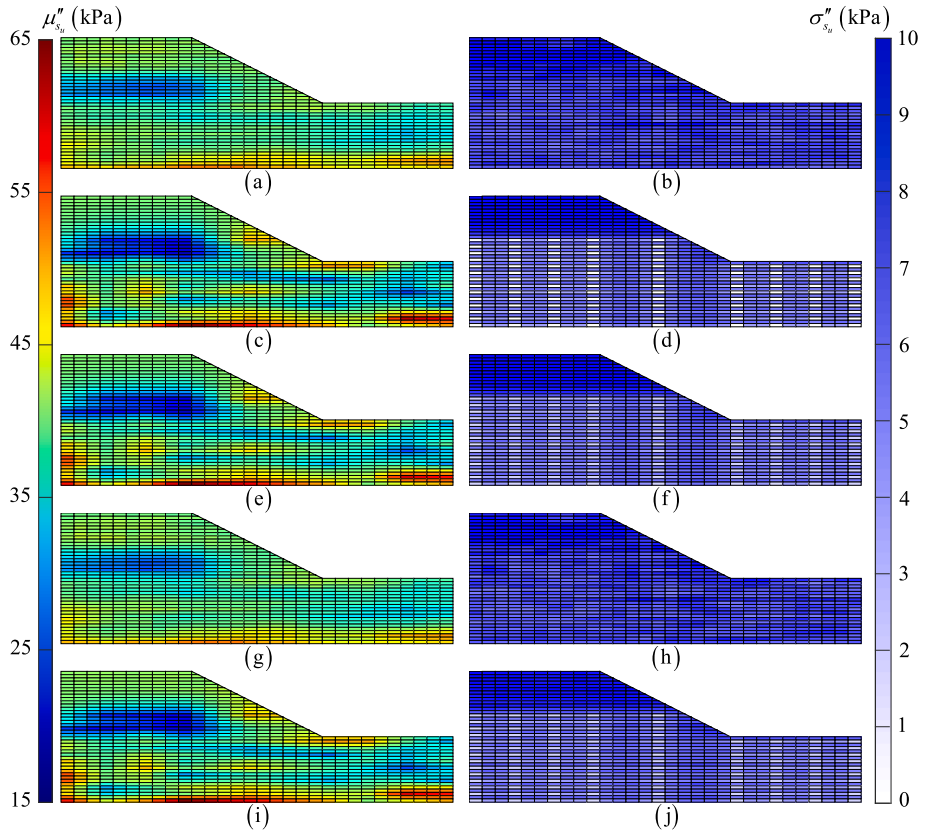

Fig. 13. Comparison of the random field realizations of posterior mean and standard deviation of s_u from different methods: (a) and (b) Integrating 110 s_u data (Original BUS method); (c) and (d) Integrating 110 s_u data (Hoffman method); (e) and (f) Integrating 110 s_u data (Improved BUS method); (g) and (h) Integrating 110 s_u data and $FS_r = 1.05$ (Original BUS method); (i) and (j) Integrating 110 s_u data and $FS_r = 1.05$ (Improved BUS method).

data presented in Fig. 6 is carried out. Similar to test case 1, a value of $\sigma_\varepsilon = 2.0$ kPa is employed. In addition, $\rho_{i,j} = 0.3$ and $\rho_{i,j} = 0.5$ are chosen, respectively, to represent the correlation structure between any two of the 14 sets of s_u data. Therefore, the theoretical correlation matrix contains 1 in the diagonal cells and $\rho_{i,j}$ in all other cells.

Following the procedures above, the proposed improved BUS method is adopted to calculate the posterior distribution of s_u. The correlation coefficients between ε_i and ε_j are then calculated from the obtained posterior samples of s_u and compared with the true correlation matrix. Referring to the calculated correlation matrix shown in Fig. 15 (a) and (b), it can be observed that the calculated values reasonably agree to the pre-set values of $\rho_{i,j} = 0.3$ and $\rho_{i,j} = 0.5$. This result demonstrates that the proposed workaround still permits sequential Bayesian model updating to improve computational efficiency and stability while preserving the correlation structure of measurement errors.

In addition, Fig. 16(a) and (b), respectively, illustrates the posterior distributions of s_u at locations A and B considering the correlation coefficients of $\rho_{i,j} = 0.3$ and $\rho_{i,j} = 0.5$ between any two of the 14 sets of s_u data (referring to Fig. 5 for the locations of A and B). Similar to the findings presented in Fig. 8, the improved BUS method also accurately calculates the posterior distributions at both locations. These distributions are smooth, and the multiple peaks associated with the results of the original BUS method are absent. These results further demonstrate that the proposed workaround is effective in handling cases involving correlation structure among field measurement data or measurement errors. Moreover, as observed from Fig. 16, the correlations among the measurement data or measurement errors have only a slight effect on the posterior distribution of s_u in this case.

5.2. Limitations and future work

There are several limitations in the present study which warrant future research. First, the cases considered in the present study involve only single-parameter random field model. The applicability of the proposed improved BUS method to multi-parameter random field models will be explored in future research.

Second, the present study deals only with two types of field information in the Bayesian model updating. Specifically, the s_u data obtained through in-situ vane shear tests are often considered as direct information. In practice, multiple types of field information are commonly available to engineers. For example, pore water pressure and displacement measurements are commonly monitored in engineering practice. The interpretation of such indirect data using the proposed improved BUS method needs also be explored.

Furthermore, the simultaneous consideration of multiple direct and indirect field information often leads to the posterior distributions of the parameters that better reflect actual engineering conditions. Future research into this aspect in the Bayesian model updating of spatially varying geomaterial parameters with multiple sources of observations is also warranted.

6. Conclusions

The present study proposes an improved BUS method based on a parallel system reliability analysis for Bayesian model updating of geomaterial parameters. The proposed improved BUS method is designed to address a technical challenge of Bayesian model updating related to the extremely small likelihood function values arising from incorporating a

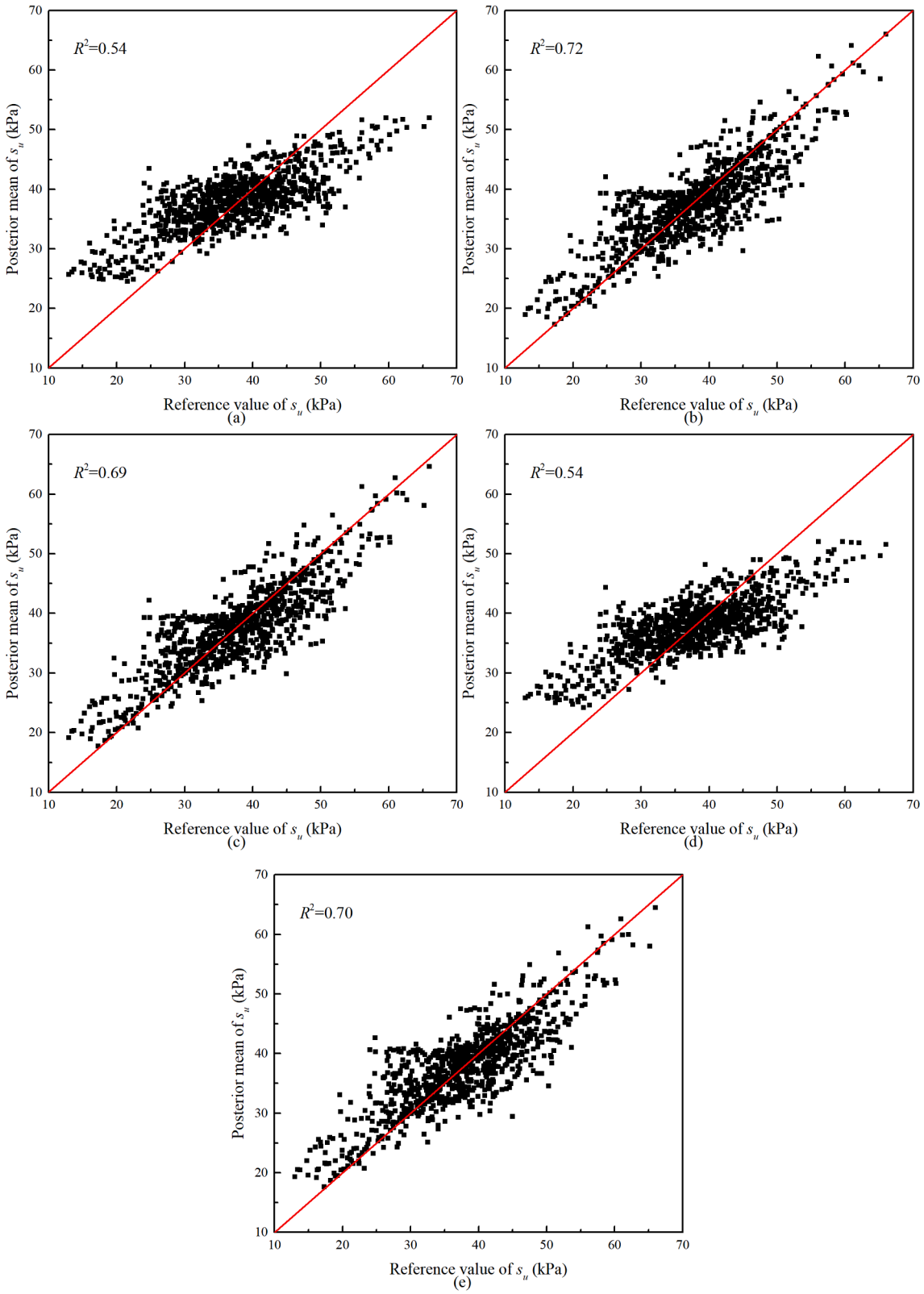

Fig. 14. Comparison of the posterior mean values and the realization of reference random field of s_u: (a) Integrating 110 s_u data (Original BUS method); (b) Integrating 110 s_u data (Hoffman method); (c) Integrating 110 s_u data (Improved BUS method); (d) Integrating 110 s_u data and $FS_r = 1.05$ (Original BUS method); (e) Integrating 110 s_u data and $FS_r = 1.05$ (Improved BUS method).

Table 3
Comparison of statistical parameters of posterior probabilities of slope failure obtained from different methods based on 10 independent repeated runs.

Data	Method	$\max(p_f)$	$\min(p_f)$	R_{p_f}	μ_{p_f}	σ_{p_f}	COV_{p_f}
110 s_u data	BUS method	0.78	0.12	0.66	0.35	0.24	0.69
	The proposed method	0.31	0.24	0.07	0.29	0.02	0.07
110 s_u data and $FS_r = 1.05$	BUS method	0.65	0.01	0.64	0.22	0.22	1.00
	The proposed method	0.18	0.09	0.09	0.13	0.03	0.23

large volume of field data, which has been increasingly common. Through a slope reliability assessment example involving spatially variable undrained shear strength, it is demonstrated that this technical issue, along with the excessive computational time and low computational accuracy, are effectively addressed by the improved BUS method. The key conclusions are summarized as below:

(i) The improved BUS method, starting from the Cholesky decomposition-based midpoint method, effectively subdivides the total failure region with a low acceptance rate into multiple sub-failure domains with high acceptance rates. This proposed configuration allows for updating one-dimensional variables at a time, and each subset simulation requires only a small number of samples. This improvement successfully reduces the generation of repeated samples occurred in the original Bayesian model updating process and enhances the sample acceptance rate.

(ii) It is demonstrated that the improved BUS method is an effective tool for incorporating a large volume of field data in the Bayesian model updating of spatially varying geomaterial parameters, and the method is sufficiently generalizable for cases involving both independent and correlated measurement data.

(iii) Compared to the original BUS method, the improved BUS method demonstrates more accurate, smooth, and practical inference of posterior probability distributions when integrating a large volume of field data (i.e., 110 sets of test data from nine boreholes), confirming the effectiveness of the proposed method.

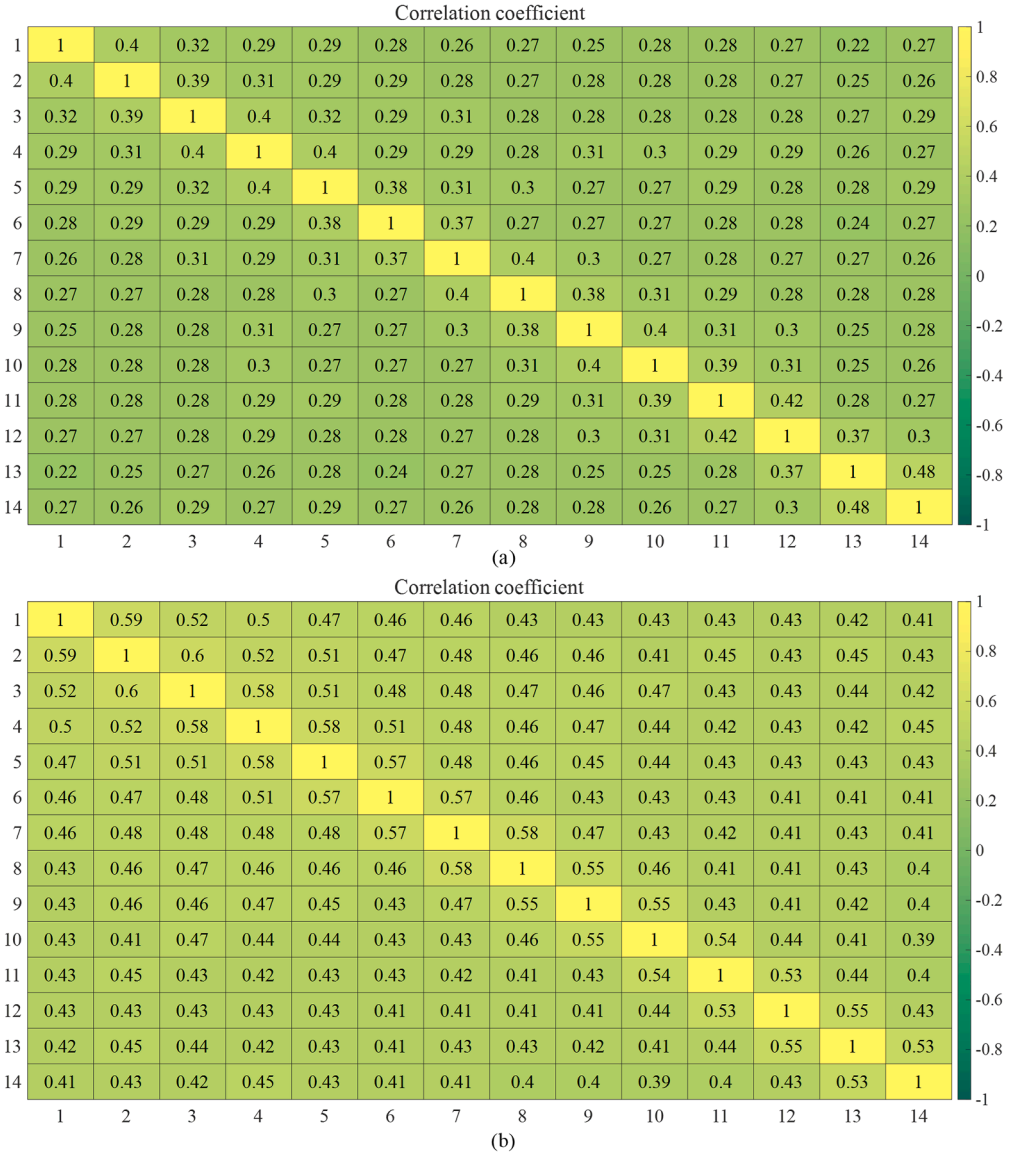

Fig. 15. Calculated correlation structures from posterior samples: (a) $\rho_{i,j} = 0.3$; (b) $\rho_{i,j} = 0.5$.

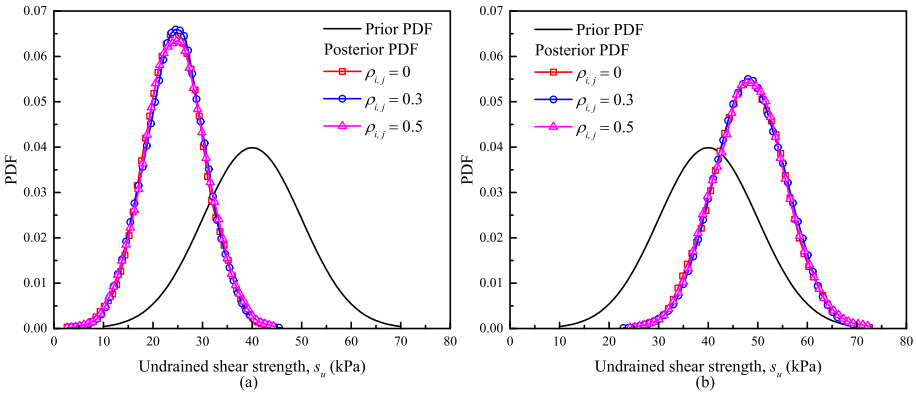

Fig. 16. Posterior PDFs of s_u at the two representative locations calculated using the proposed workaround based on $\rho_{i,j} = 0.3$ and $\rho_{i,j} = 0.5$, respectively: (a) location *A*; (b) location *B*.

CRediT authorship contribution statement

Shui-Hua Jiang: Writing – review & editing, Validation, Supervision, Software, Resources, Project administration, Methodology, Investigation, Funding acquisition, Conceptualization. **Hong-Peng Hu:** Writing – original draft, Visualization, Investigation, Formal analysis. **Ze Zhou Wang:** Writing – review & editing, Validation, Supervision, Methodology, Funding acquisition, Formal analysis.

Declaration of competing interest

The authors declare that they have no known competing financial interests or personal relationships that could have appeared to influence the work reported in this paper.

Data availability

Data will be made available on request.

Acknowledgments

This work was supported by the Natural Science Foundation of Jiangxi Province (Grant Nos. 20242ACB221001, 20224ACB204019 and 20232ACB204031), National Natural Science Foundation of China (Grant Nos. 52179103, 52222905 and 42272326) and European Union's Horizon 2020 research and innovation program under the Marie Skłodowska-Curie grant agreement (Grant No. 101034337). The financial support is gratefully acknowledged.

Appendix A

The BUS method constructs a failure region Ω_{acc} by introducing an uniformly distributed variable in the interval [0, 1.0], which transforms the Bayesian model updating problem into an equivalent reliability problem. The proposed improved BUS method subdivides the original failure domain with a low acceptance rate into several sub-failure domains according to Eq. (11). In this way, the posterior distribution $f'_X(\boldsymbol{x})$ can be formulated as

$$f'_X(\boldsymbol{x}) = \frac{\int_{U\in\Omega_{acc}} f'(\boldsymbol{x})dU}{\int_{[\boldsymbol{x},U]\in\Omega_{acc}} f'(\boldsymbol{x})dUd\boldsymbol{x}} = \frac{\int_0^1 I^{acc}([\boldsymbol{x},U]\in\Omega_{acc})f'_X(\boldsymbol{x})dU}{\int_X\int_0^1 I^{acc}([\boldsymbol{x},U]\in\Omega_{acc})f'_X(\boldsymbol{x})dUd\boldsymbol{x}} \tag{A1}$$

Based on Eq. (11), Eq. (A1) can be rewritten as

$$\begin{aligned} f'_X(\boldsymbol{x}) &= \frac{\int_{U_{n_d}\in\Omega_{acc}^{n_d}}\cdots\int_{U_1\in\Omega_{acc}^1} f'_X(\boldsymbol{x})dU_1\cdots dU_{n_d}}{\int_{[\boldsymbol{x},U_{n_d}]\in\Omega_{acc}^{n_d}}\cdots\int_{[\boldsymbol{x},U_1]\in\Omega_{acc}^1} f'_X(\boldsymbol{x})dU_1\cdots dU_{n_d}d\boldsymbol{x}} \\ &= \frac{\int_0^1 I_{n_d}^{acc}([\boldsymbol{x},U_{n_d}]\in\Omega_{acc}^{n_d})\cdots[\int_0^1 I_1^{acc}([\boldsymbol{x},U_1]\in\Omega_{acc}^1)]f'_X(\boldsymbol{x})dU_1]\cdots dU_{n_d}}{\int_X\int_0^1 I_{n_d}^{acc}([\boldsymbol{x},U_{n_d}]\in\Omega_{acc}^{n_d})\cdots[\int_0^1 I_1^{acc}([\boldsymbol{x},U_1]\in\Omega_{acc}^1)]f'_X(\boldsymbol{x})dU_1]\cdots dU_{n_d}d\boldsymbol{x}} \end{aligned} \tag{A2}$$

As proved by Wang and Shafieezadeh [40], the numerator of Eq. (A2) can be evaluated as

$$\begin{aligned} \int_{U_{n_d}\in\Omega_{acc}^{n_d}}\cdots\int_{U_1\in\Omega_{acc}^1} f'_X(\boldsymbol{x})dU_1\cdots dU_{n_d} &= \int_0^{c_{n_d}W_{n_d}(\boldsymbol{x})}\cdots\int_0^{c_1W_1(\boldsymbol{x})} f'_X(\boldsymbol{x})dU_1\cdots dU_{n_d} \\ &= \int_0^{c_{n_d}W_{n_d}(\boldsymbol{x})}\cdots\int_0^{c_2W_2(\boldsymbol{x})} c_1W_1(\boldsymbol{x})f'_X(\boldsymbol{x})dU_2\cdots dU_{n_d} \\ &= f'_X(\boldsymbol{x})\prod_{k=1}^{n_d}[c_kW_k(\boldsymbol{x})] = L(\boldsymbol{x})f'_X(\boldsymbol{x})\prod_{k=1}^{n_d}c_k \end{aligned} \tag{A3}$$

The denominator of Eq. (A2) can be evaluated as

$$
\begin{aligned}
&\int_{[\boldsymbol{x},U_{n_d}]\in\Omega_{acc}^{n_d}}\cdots\int_{[\boldsymbol{x},U_1]\in\Omega_{acc}^{1}} f_X'(\boldsymbol{x})dU_1\cdots dU_{n_d}d\boldsymbol{x}\\
&=\int_X\int_0^1 I_{n_d}^{acc}([\boldsymbol{x},U_{n_d}]\in\Omega_{acc}^{n_d})\cdots\left[\int_0^1 I_1^{acc}([\boldsymbol{x},U_1]\in\Omega_{acc}^{1})f_X'(\boldsymbol{x})dU_1\right]\cdots dU_{n_d}d\boldsymbol{x}\\
&=\int_X\int_0^1 I_{n_d}^{acc}\left[U_{n_d}\le c_{n_d}W_{n_d}(\boldsymbol{x})\right]\cdots\left\{\int_0^1 I_1^{acc}[U_1\le c_1W_1(\boldsymbol{x})]f_X'(\boldsymbol{x})dU_1\right\}\cdots dU_{n_d}d\boldsymbol{x}\\
&=\int_X f_X'(\boldsymbol{x})\prod_{k=1}^{n_d}[c_kW_k(\boldsymbol{x})]d\boldsymbol{x}=\prod_{k=1}^{n_d}c_k\left(\prod_{k=1}^{n_d}c_k\right)\int_X f_X'(\boldsymbol{x})\prod_{k=1}^{n_d}[W_k(\boldsymbol{x})]d\boldsymbol{x}\\
&=\prod_{k=1}^{n_d}c_k\int_X f_X'(\boldsymbol{x})L(\boldsymbol{x})d\boldsymbol{x}
\end{aligned}
\tag{A4}
$$

In this way, Eq. (A2) can be simplified as

$$
f_X''(\boldsymbol{x})=\frac{L(\boldsymbol{x})f_X'(\boldsymbol{x})}{\int_X L(\boldsymbol{x})f_X'(\boldsymbol{x})d\boldsymbol{x}} \tag{A5}
$$

This confirms that the division in Eq. (11) can keep the properties of the physical problem.

References

[1] Ang AH, Tang WH. Probability concepts in engineering: emphasis on applications to civil and environmental engineering. 2nd ed. Hoboken, New Jersey: John Wiley and Sons; 2007.
[2] Asaoka A, A-Grivas D. Spatial variability of the undrained strength of clays. J Geotech Eng Div 1982;108(5):743–56.
[3] Au SK, Beck JL. Estimation of small failure probabilities in high dimensions by subset simulation. Probab Eng Mech 2001;16(4):263–77.
[4] Betz W, Papaioannou I, Beck JL, Straub D. Bayesian inference with subset simulation: strategies and improvements. Comput Methods Appl Mech Eng 2018; 331:72–93.
[5] Ching J, Wang JS. Application of the transitional Markov chain Monte Carlo algorithm to probabilistic site characterization. Eng Geol 2016;203:151–67.
[6] Christian JT, Ladd CC, Baecher GB. Reliability applied to slope stability analysis. J Geotech Eng 1994;120(12):2180–207.
[7] Deng JH, Lee CF. Displacement back analysis for a steep slope at the Three Gorges Project site. Int J Rock Mech Min Sci 2001;38(2):259–68.
[8] Der Kiureghian A, Ke JB. The stochastic finite element method in structural reliability. Probab Eng Mech 1988;3(2):83–91.
[9] Depina I, Oguz EA, Thakur V. Novel Bayesian framework for calibration of spatially distributed physical-based landslide prediction models. Comput Geotech 2020;125: 103660.
[10] Dodt MB, Kitahara M, Broggi M, Michael B. Comparison of state of the art sampling-based Bayesian Updating techniques. In Proceedings of the 8th International Symposium on Reliability Engineering and Risk Management 2022: (pp. 59-66). Research Publishing (S) Pte Ltd; Singapore.
[11] Ering P, Sivakumar Babu GL. Probabilistic back analysis of rainfall induced landslide-A case study of Malin landslide, India. Eng Geol 2016;208:154–64.
[12] Feng K, Lu Z, Wang J, He P, Dai Y. Efficient reliability updating methods based on Bayesian inference and sequential learning Kriging. Struct Saf 2023;104:102366.
[13] Gong W, Juang CH, Martin II JR, Tang HM, Wang QQ, Huang HW. Probabilistic analysis of tunnel longitudinal performance based upon conditional random field simulation of soil properties. Tunn Undergr Space Technol 2018;73:1–14.
[14] Harris SJ, Orense RP, Itoh K. Back analyses of rainfall-induced slope failure in Northland Allochthon formation. Landslides 2012;9:349–56.
[15] Hoffman Y, Ribak E. Constrained realizations of Gaussian fields-A simplealgorithm. Astrophys J, Part 2-Letters, 1991;380:L5-L8.
[16] Jerez DJ, Jensen HA, Beer M. An effective implementation of reliability methods for Bayesian model updating of structural dynamic models with multiple uncertain parameters. Reliab Eng Syst Safe 2022;225:108634.
[17] Jiang SH, Papaioannou I, Straub D. Bayesian updating of slope reliability in spatially variable soils with in-situ measurements. Eng Geol 2018;239:310–20.
[18] Jiang SH, Huang J, Huang F, Yang J, Yao C, Zhou CB. Modelling of spatial variability of soil undrained shear strength by conditional random fields for slope reliability analysis. App Math Model 2018;63:374–89.
[19] Jiang SH, Huang J, Qi XH, Zhou CB. Efficient probabilistic back analysis of spatially varying soil parameters for slope reliability assessment. Eng Geol 2020; 271:105597.
[20] Jiang SH, Huang J, Griffiths DV, Deng ZP. Advances in reliability and risk analyses of slopes in spatially variable soils: A state-of-the-art review. Comput Geotech 2022;141:104498.
[21] Jiang SH, Liu X, Wang ZZ, Li DQ, Huang J. Efficient sampling of the irregular probability distributions of geotechnical parameters for reliability analysis. Struct Saf 2023;101:102309.
[22] Kamariotis A, Sardi L, Papaioannou I, Chatzi E, Straub D. On off-line and on-line Bayesian filtering for uncertainty quantification of structural deterioration. Data-Centric Eng 2023;4:e17.
[23] Kasama K, Whittle AJ, Zen K. Effect of spatial variability on the bearing capacity of cement-treated ground. Soils Found 2012;52(4):600–19.
[24] Lee SH, Song J. System identification of spatial distribution of structural parameters using modified transitional Markov chain Monte Carlo method. J Eng Mech 2017;143(9):04017099.
[25] Li D, Chen Y, Lu W, Zhou C. Stochastic response surface method for reliability analysis of rock slopes involving correlated non-normal variables. Comput Geotech 2011;38(1):58–68.
[26] Li DQ, Jiang SH, Cao ZJ, Zhou W, Zhou CB, Zhang LM. A multiple response-surface method for slope reliability analysis considering spatial variability of soil properties. Eng Geol 2015;187:60–72.
[27] Liu X, Wang Y, Koo RC, Kwan JS. Development of a slope digital twin for predicting temporal variation of rainfall-induced slope instability using past slope performance records and monitoring data. Eng Geol 2022;308:106825.
[28] Liu X, Ma G, Rezaniaa M, Li X, Jiang SH. An improved BUS approach for bayesian inverse analysis of soil parameters incorporating extensive field data. Comput Geotech 2024;174:106641.
[29] Liu Y, Liu C, Xu W, Cai S, Ren W. Efficient probabilistic back analysis of spatially varying soil parameters based on monitored displacements. Arab J Geosci 2022;15 (9):817.
[30] Ouyang J, Liu Y. Model updating for slope stability assessment in spatially varying soil parameters using multi-type observations. Mech Syst Sig Process 2022;171: 108906.
[31] Papaioannou I, Straub D. Learning soil parameters and updating geotechnical reliability estimates under spatial variability. Georisk 2017;11(1):116–28.
[32] Papaioannou I, Betz W, Zwirglmaier K, Straub D. MCMC algorithms for subset simulation. Probab Eng Mech 2015;41:89–103.
[33] Phoon KK, Kulhawy FH. Characterization of geotechnical variability. Can Geotech J 1999;36(4):612–24.
[34] Santoso AM, Phoon KK, Quek ST. Modified Metropolis-Hastings algorithm with reduced chain correlation for efficient subset simulation. Probab Eng Mech 2011; 26(2):331–41.
[35] Simoen E, Papadimitriou C, Lombaert G. On prediction error correlation in Bayesian model updating. J Sound Vib 2013;332(18):4136–52.
[36] Straub D, Papaioannou I. Bayesian updating with structural reliability methods. J Eng Mech 2015;141(3):04014134.
[37] Sun Y, Huang J, Jin W, Sloan SW, Jiang Q. Bayesian updating for progressive excavation of high rock slopes using multi-type monitoring data. Eng Geol 2019; 252:1–13.
[38] Wang L, Hwang JH, Luo Z, Juang CH, Xiao J. Probabilistic back analysis of slope failure–a case study in Taiwan. Comput Geotech 2013;51:12–23.
[39] Wang Y, Cao Z, Au SK. Practical reliability analysis of slope stability by advanced Monte Carlo simulations in a spreadsheet. Can Geotech J 2011;48(1):162–72.
[40] Wang Z, Shafieezadeh A. Highly efficient Bayesian updating using metamodels: An adaptive Kriging based approach. Struct Saf 2020;84:101915.
[41] Wang Z, Shafieezadeh A. Bayesian updating with adaptive, uncertainty-informed subset simulations: High-fidelity updating with multiple observations. Reliab Eng Syst Saf 2023;230:108901.
[42] Wu SH, Ou CY, Ching J, Juang CH. Reliability-based design for basal heave stability of deep excavations in spatially varying soils. J Geotech Geoenviron Eng 2012;138(5):594–603.

[43] Zhang H, Song L, Bai G. Active Kriging-Based Adaptive Importance Sampling for Reliability and Sensitivity Analyses of Stator Blade Regulator. CMES-Comp Model Eng 2023;134(3):1871–97.
[44] Zhang LL, Zhang J, Zhang LM, Tang WH. Back analysis of slope failure with Markov chain Monte Carlo simulation. Comput Geotech 2010;37(7–8):905–12.
[45] Zhang L, Wu F, Wei X, Yang HQ, Fu S, Huang J, et al. Polynomial chaos surrogate and bayesian learning for coupled hydro-mechanical behavior of soil slope. Rock Mechanics Bulletin 2023;2(1):100023.
[46] Zhao ZT, Mu HQ, Yuen KV. Probability density function modelling and credible region construction for multivariate, asymmetric, and multimodal distributions of geotechnical data. Struct Saf 2024;107:102429.
[47] Jiang SH, Zhu GY, Wang ZZ, Huang ZT, Huang J. Data augmentation for CNN-based probabilistic slope stability analysis in spatially variable soils. Comput Geotech 2023;160:105501.